Right-angled polyhedra and alternating links

ABHIJIT CHAMPANERKAR
ILYA KOFMAN
JESSICA S PURCELL

To any prime, alternating link, we associate a collection of hyperbolic right-angled ideal polyhedra by relating geometric, topological and combinatorial methods to decompose the link complement. The sum of the hyperbolic volumes of these polyhedra is a new geometric link invariant, which we call the right-angled volume of the alternating link. We give an explicit procedure to compute the right-angled volume from any alternating link diagram, and prove that it is a new lower bound for the hyperbolic volume of the link.

1 Introduction

Right-angled structures have featured in many striking results in 3–manifold geometry, topology and group theory. Alternating knot complements decompose into pieces with essentially the same combinatorics as the alternating diagram, so the hyperbolic geometry of alternating knots is closely related to their diagrams. Therefore, it is natural to ask: Which alternating links are right-angled? In other words, when does the link complement with the complete hyperbolic structure admit a decomposition into ideal hyperbolic right-angled polyhedra? Surprisingly, besides the Whitehead and Borromean links, only two alternating links are known to be right-angled; see Gan [14]. In Section 5.5, we conjecture that, whether alternating or not, there does not exist a right-angled knot.

However, we can obtain right-angled structures from alternating diagrams, which do not give the complete hyperbolic structure, but nevertheless provide useful and computable geometric link invariants. These turn out to be related to previous geometric constructions obtained from alternating diagrams, and below we relate these constructions to each other in new ways.

Specifically, we associate a set of hyperbolic right-angled ideal polyhedra to any reduced, prime, alternating link diagram. We prove that these polyhedra can be described equivalently from the following geometric, topological and combinatorial perspectives. This equivalence implies that such a set of right-angled polyhedra is a link invariant, whose volume sum we call the *right-angled volume* $\mathrm{vol}^\perp(K)$ of the alternating link K. We prove that this new geometric link invariant is a lower bound for the hyperbolic volume of the link, and is asymptotically sharp for certain sequences of knots and links.

Geometry

The *guts* of a 3–manifold cut along an essential surface is the union of all the hyperbolic pieces in its JSJ decomposition. Lackenby [19], building on work of Thurston [33], Agol [1] and Menasco [22], described such a geometric decomposition of the complement of any alternating link by cutting along its two checkerboard surfaces. In [8], we determined explicitly the guts of the manifolds obtained from alternating links with certain extra hypotheses, cut along *both* checkerboard surfaces. In Section 2, we again analyze the guts of these manifolds, but we remove the extra hypotheses on the alternating links, and we construct the associated hyperbolic right-angled *guts polyhedra*.

Topology

Bonahon and Siebenmann [6], building on work of Conway [12] and Montesinos [26], defined a *characteristic splitting* of any link diagram along Conway spheres into arborescent and nonarborescent parts. In the double-branched cover of the link, the arborsescent part is covered by a graph manifold, and the nonarborsescent part by a hyperbolic manifold. Menasco and Thistlethwaite [23; 24; 32; 31] showed that, up to flypes, an alternating diagram can be decomposed only in limited ways along invariant Conway spheres into alternating tangles. Thistlethwaite [31] used such tangles to completely describe the characteristic splitting of any alternating link diagram. In Section 3, we use Thistlethwaite's results to build *tangle polyhedra* associated with the nonarborescent part of an alternating link.

Combinatorics

Right-angled polyhedra are natural hyperbolic "bricks" which have been used to construct hyperbolic 3–manifolds. In 1931, Löbell [20] constructed the first example

of a closed orientable hyperbolic 3–manifold by gluing eight copies of the right-angled 14–hedron. Andreev's theorem (Theorem 4.7 below) implies that, up to isometry, a hyperbolic right-angled ideal polyhedron is uniquely determined by its combinatorial type. In Section 4, we define rational reduction of an alternating link diagram, and then determine its diagrammatic splitting into *Andreev polyhedra*.

One main result of this paper is the somewhat surprising fact that the three polyhedra, obtained from now-classic geometric, topological and combinatorial methods, actually give the same link invariant for alternating links!

Theorem 4.11 *The Andreev polyhedra are identical to the tangle polyhedra and the guts polyhedra.*

Right-angled volume

In Section 5, we define the right-angled volume $\text{vol}^\perp(K)$ of an alternating link K as the sum of the hyperbolic volumes of these right-angled polyhedra. It gives a new geometric link invariant for alternating links.

Theorem 5.3 *For any hyperbolic alternating link L with hyperbolic volume $\text{vol}(L)$,*

$$\text{vol}^\perp(L) \leq \text{vol}(L).$$

Morover, we show the bound is asymptotically sharp: there exist many sequences of alternating links K_n such that

$$\lim_{n\to\infty} \frac{\text{vol}^\perp(K_n)}{\text{vol}(K_n)} = 1.$$

To compare $\text{vol}^\perp(L)$ with other volume bounds, we exhibit examples for which $\text{vol}^\perp(L)$ beats the best previous lower bounds, given by Agol, Storm and Thurston [2] and Lackenby [19], by a factor of two. However, for any Montesinos link, which may have arbitrarily large volume, $\text{vol}^\perp(L) = 0$. Thus, as a lower volume bound, $\text{vol}^\perp(L)$ should be used together with other bounds. We discuss this further in Section 5.4.

Acknowledgements

2 Geometry

2.1 Background on guts

By work of Menasco, if a link has a reduced, prime, alternating diagram that is not the diagram of a $(2, q)$–torus link, then the link complement is hyperbolic. However, it can be difficult to determine geometric information directly from a diagram.

We will cut a 3–manifold along an essential surface and consider its JSJ decomposition [16; 17; 18], which cuts the 3–manifold into components consisting of I–bundles, Seifert-fibered pieces and *guts*. To describe the guts, we need to set up some definitions and notation. We will mainly consider 3–manifolds M that admit a finite-volume hyperbolic structure. We may view such a manifold as the interior of a compact manifold $\overline{M}$ with torus boundary components. The fact that M is hyperbolic means it admits a hyperbolic structure $M \cong \mathbb{H}^3 / \Gamma$, where Γ is a discrete subgroup of $\mathrm{PSL}(2, \mathbb{C})$. Under this structure, any closed curve in a neighborhood of $\partial \overline{M}$ is isotopic to a *parabolic* element of Γ.

We view M as an open manifold without boundary, but at times it will be more convenient to consider the compact manifold $\overline{M}$. In the case of a link complement, $M = S^3 - L$, the compact manifold $\overline{M}$ is homeomorphic to $S^3 - N(L)$, where $N(L)$ denotes an open regular neighborhood of L in S^3. Then $\partial \overline{M}$ is a collection of tori. These form the *parabolic locus* of $\overline{M}$. More generally, the parabolic locus λ of a compact 3–manifold $\overline{M}$ will consist of annuli and tori in $\partial \overline{M}$. When we want to carefully keep track of the parabolic locus, we write the manifold as a pair $(\overline{M}, \lambda)$. For our link example, we have the pair $(S^3 - N(L), \partial N(L))$.

Now, we wish to cut a 3–manifold M along an essential surface S. When we view M as an open manifold, then S will be a properly embedded open surface, homeomorphic to the interior of a compact surface $\overline{S}$ with boundary on $\partial \overline{M}$. Let $M \backslash\!\backslash S$ denote the closure (in M) of the manifold obtained by removing a regular neighborhood of S from M. The boundary of $M \backslash\!\backslash S$ is homeomorphic to $\widetilde{S} = \partial N(S)$, the double cover of S.

On the other hand, we may also express this information in terms of a pair. If $\overline{M}$ has parabolic locus $\partial \overline{M}$ consisting of tori, then we express the cut manifold as a pair $(\overline{M} \backslash\!\backslash \overline{S}, \partial(\overline{M}) \backslash\!\backslash \partial \overline{S})$. Note that the parabolic locus will now include annular components.

A pair $(\overline{M}, \lambda)$ is called a *pared acylindrical 3–manifold* if $\overline{M}$ is a compact, irreducible, atoroidal manifold with boundary (such as $S^3 - N(L)$ or $\overline{M} \backslash\backslash \overline{S}$) and $\lambda \subset \partial \overline{M}$ is a union of incompressible annuli and tori such that every map $(S^1 \times I, S^1 \times \partial I) \to (\overline{M}, \partial \overline{M} - \lambda)$ that is π_1–injective deforms as a map of pairs into λ. Denote $\partial \overline{M} - \lambda$ by $\partial_0 \overline{M}$. Thurston showed that a pared acylindrical 3–manifold admits a hyperbolic metric with totally geodesic boundary $\partial_0 M$ and parabolic locus λ [27].

For M an open 3–manifold and S an essential surface, the *guts* of $M \backslash\backslash S$, denoted by $\mathrm{guts}(M \backslash\backslash S)$, is the union of all components in the JSJ decomposition of $M \backslash\backslash S$ that admit a hyperbolic structure. In terms of the notation of pared manifolds, let $(\overline{M}, \partial \overline{M})$ denote the pair corresponding to M. Let A denote the union of essential annuli in $M \backslash\backslash S$. Let M_1 be a hyperbolic component of $(M \backslash\backslash S) \backslash\backslash A$, so M_1 is a component of $\mathrm{guts}(M \backslash\backslash S)$. It is associated to a pair $(\overline{M}_1, \lambda_1)$, where $\overline{M}_1$ is the union of M_1 along with its boundary as a subset of $\overline{M}$, and λ_1 consists of $\partial \overline{M} \cap \partial M_1$ as well as any component of $\widetilde{A} \cap M_1$. That is, when we take the JSJ decomposition of a 3–manifold, all essential annuli that we cut along to form the decomposition become part of the parabolic locus of the guts.

2.2 Checkerboard decomposition

Suppose L is a link that admits a reduced, prime, alternating diagram. Its two checkerboard surfaces are essential [5; 19], and so we may follow the procedure outlined above and cut along a checkerboard surface S, obtaining the guts of $(S^3 - L) \backslash\backslash S$. Indeed, we will use a doubling procedure to cut along both checkerboard surfaces.

Let L be a link with reduced, prime, alternating diagram, and associated checkerboard surfaces B and R. It is well known that cutting $S^3 - L$ along both B and R simultaneously decomposes it into two identical (topological) ideal polyhedra [22]. For an alternating link, each of the two ideal polyhedra is obtained by taking edges and ideal vertices corresponding to the diagram graph of the link. Call one of these ideal polyhedra the *checkerboard polyhedron* associated to the link diagram.

Instead of cutting along both surfaces simultaneously, we cut along the two surfaces separately and consider the guts. Let M_B denote the 3–manifold consisting of the guts of $(S^3 - L) \backslash\backslash B$, and M_R the guts of $(S^3 - L) \backslash\backslash R$; ie

$$M_B = \mathrm{guts}((S^3 - L) \backslash\backslash B), \quad M_R = \mathrm{guts}((S^3 - L) \backslash\backslash R).$$

The boundary $\partial_0 M_B$ consists of $M_B \cap \widetilde{B}$, and similarly $\partial_0 M_R$ consists of $M_R \cap \widetilde{R}$. The parabolic locus of each consists of remnants of the link and essential annuli that we cut along to form the guts.

Let $D(M_B)$ denote the double of M_B along the surface $\partial_0 M_B$. This manifold admits a hyperbolic structure in which $\partial_0 M_B$ is totally geodesic, and similarly for $D(M_R)$.

In [8, Lemma 4.8], we showed that the surface $R \cap M_B$ doubles to give an essential surface DR in $D(M_B)$. Similarly, $B \cap M_R$ doubles to give an essential surface DB in $D(M_R)$. Thus, we may cut along these surfaces, and find the guts of the resulting pieces. That is, consider the manifold $\mathrm{guts}(D(M_B) \backslash\backslash DR)$. This is a 3–manifold with boundary consisting of $\widetilde{DR} \cap \mathrm{guts}(D(M_B) \backslash\backslash DR)$. Its double $D\big(\mathrm{guts}(D(M_B) \backslash\backslash DR)\big)$ therefore admits a hyperbolic structure in which $\widetilde{DR} \cap \mathrm{guts}(D(M_B) \backslash\backslash DR)$ is totally geodesic.

In [8], we showed that, under certain hypotheses on L, $\mathrm{guts}(D(M_B) \backslash\backslash DR)$ is the entire manifold $D(M_B) \backslash\backslash DR$. In this case, the double $D\big(\mathrm{guts}(D(M_B) \backslash\backslash DR)\big)$ is built by gluing eight copies of the original checkerboard polyhedron obtained by cutting $S^3 - L$ along B and R. We now drop the restrictions on L from [8].

Let $D\big(D((S^3 - L) \backslash\backslash B) \backslash\backslash DR\big)$ denote the manifold obtained first by cutting along B, then doubling, then cutting along DR and doubling. We will show:

Proposition 2.1 *The manifold $D\big(\mathrm{guts}(D(M_B) \backslash\backslash DR)\big)$ is homeomorphic to*

- *the guts of the manifold $D\big(D((S^3 - L) \backslash\backslash B) \backslash\backslash DR\big)$,*
- *the guts of the manifold $D\big(D((S^3 - L) \backslash\backslash R) \backslash\backslash DB\big)$,*
- *$D\big(\mathrm{guts}(D(M_R) \backslash\backslash DB)\big)$.*

Moreover, all four manifolds are built by gluing eight copies of a collection of polyhedra, obtained by cutting the checkerboard polyhedron along normal squares and collapsing each normal square boundary to an ideal vertex.

A *normal square* is a disk properly embedded in the checkerboard polyhedron that meets exactly four faces of the polyhedron in *normal form* — basically transversely and without backtracking; see for example [19], or [13, Definition 3.15] for a precise definition of normal form, or Lemma 2.5 below for a description of normal squares in a checkerboard polyhedron. Note that we will use the term *square* below to refer to (normal) squares in a polyhedron as well as to corresponding curves in a diagram, ie

curves that meet the diagram exactly four times, using the correspondance between the diagram and the checkerboard polyhedra noted above.

Definition 2.2 (guts polyhedra) Let L be a link with a reduced, prime, alternating diagram. The *guts polyhedra* associated to the diagram are the ideal polyhedra obtained from Proposition 2.1 by taking one of the eight copies of polyhedra making up the guts of

$$D\big(D((S^3 - L)\backslash\!\backslash B)\backslash\!\backslash DR\big).$$

Alternatively, it is obtained by cutting the checkerboard polyhedron along normal squares required for that proposition, and discarding Seifert-fibered or I–bundle components.

Our main interest in studying the guts polyhedra is the following result:

Theorem 2.3 *The unique hyperbolic structure on $D\big(\mathrm{guts}(D(M_B)\backslash\!\backslash DR)\big)$ induces a hyperbolic structure on the guts polyhedra in which the red and blue faces are totally geodesic, with red faces meeting blue at right angles.*

The rest of this section gives the proofs of Proposition 2.1 and Theorem 2.3.

We will prove a sequence of results that will help us understand the form of the guts polyhedra, and how to identify them in a given link complement. First, we present an example.

Example 2.4 (Borromean rings) When L is the standard reduced alternating diagram of the Borromean rings, Thurston showed that the checkerboard polyhedron associated with $S^3 - L$ is a regular ideal octahedron [33]. Checkerboard color the faces blue and red. In this case, $(S^3 - L)\backslash\!\backslash B$ is obtained by cutting two copies of the regular ideal octahedron along blue faces. The result is hyperbolic with geodesic boundary, and so its guts, M_B, is built of two copies of the regular ideal octahedron. When we double, $D(M_B)$ is made of four copies of the regular ideal octahedron. Now cut along DR. This cuts along red faces, but again the manifold, built of four regular ideal octahedra, is hyperbolic with geodesic boundary. Hence, its guts is a manifold made up of the four octahedra, and its double is made up of eight octahedra. Tracing back through the definition, in this case the guts polyhedra is the single regular ideal octahedron. It agrees with the checkerboard polyhedron.

In order to identify guts polyhedra, we need to identify the guts of manifolds obtained from the original link complement. In order to identify guts, we need to identify tori and annuli of the JSJ decomposition of the cut manifold. Because we are assuming we begin with a hyperbolic link, in fact there will be no essential tori, and we need only to identify essential annuli. The following lemma gives the relationship of the essential annuli to the normal squares of Proposition 2.1.

Lemma 2.5 *Let M be an irreducible, boundary irreducible 3–manifold and S an essential surface properly embedded in M such that $M \backslash\backslash S$ can be decomposed into a finite number of 4–valent checkerboard polyhedra with red and blue faces, where blue faces map to $\widetilde{S}$. Let A be an essential annulus in $M \backslash\backslash S$ with boundary components $\partial A \subset \widetilde{S}$. Then A can be isotoped into normal form with respect to the checkerboard polyhedra; ie:*

- *A meets the polyhedra in disks.*
- *Each such disk is a square: it has exactly four sides running through four faces, with opposite sides in faces of the same color, and it meets four edges and no vertices of the polyhedron.*
- *Each side of a square is an arc in a face of the polyhedron with endpoints on distinct edges.*

Proof The fact that such an essential surface can be put into normal form is well known; for example it is noted in [19; 13]. By an Euler characteristic argument, such an annulus decomposes into normal squares. □

Lemma 2.6 *For L a link with a reduced, prime, alternating diagram, and notation as above, both the manifolds $D(M_B)$ and $D\big(\mathrm{guts}(D(M_B) \backslash\backslash DR)\big)$ have a decomposition into a finite collection of 4–valent ideal polyhedra that admit a checkerboard coloring, red and blue. Each polyhedron in the collection can be identified with a subset of the checkerboard polyhedron of the diagram of L, obtained by cutting the checkerboard polyhedron along a normal square, and then collapsing the normal square to a new ideal vertex. Each red (blue) face is a subset of a red (blue) face of the checkerboard polyhedron. Finally, $D\big(\mathrm{guts}(D(M_B) \backslash\backslash DR)\big)$ is made up of eight copies of a finite collection of such polyhedra.*

Proof We apply Lemma 2.5 twice. If A is an essential annulus in $(S^3 - L) \backslash\backslash B$, then A meets the checkerboard polyhedra of $S^3 - L$ in a collection of normal squares, by

that lemma. Thus, when we cut along A, we split the checkerboard polyhedra into new polyhedra, each a subset of the checkerboard polyhedra. Because A becomes part of the parabolic locus in M_B, we then collapse the squares that came from A into ideal vertices. Thus, after the first step of taking the guts, we have split checkerboard polyhedra into new ideal polyhedra with a red–blue checkerboard coloring as described. Discard polyhedra that give I–bundle or Seifert-fibered pieces, and double the result along the blue faces. This doubles the number of polyhedra, and gives the manifold $D(M_B)$. So $D(M_B)$ is built of 4–valent polyhedra that satisfy the conclusions of the first part of the lemma. The surface DR is the image of the red faces of these polyhedra under the gluing.

For the second step, we cut along $DR \cap D(M_B)$, which is equivalent to cutting the 4–valent polyhedra of $D(M_B)$ along red faces. Then we find essential annuli in $D(M_B) \backslash\backslash DR$. Any such annulus can be put into normal form with respect to the polyhedra for $D(M_B)$, and by Lemma 2.5 it meets the polyhedra of $D(M_B)$ in squares. Again these cut the polyhedra into new checkerboard colored polyhedra, and after collapsing the squares to ideal vertices we have 4–valent ideal polyhedra as claimed.

For the final statement, we count the number of copies of polyhedra. Cutting along normal squares to obtain M_B and then doubling gives four copies of polyhedra obtained by cutting the original checkerboard polyhedron along normal squares. Cutting these along normal squares and then doubling gives eight copies of new polyhedra obtained from the original by cutting along normal squares.   □

2.3 Identifying the guts

In the process of proving the rest of Proposition 2.1 and Theorem 2.3, we will explicitly determine the guts from a reduced, prime, alternating diagram of the link L. This will allow us to explicitly find the guts polyhedra. In particular, not every polyhedron obtained by cutting the checkerboard polyhedron along a normal square will be part of the guts. First, not every normal square is necessarily a square in the decomposition of an essential annulus into normal form as in Lemma 2.5. Second, some polyhedra resulting may be part of the I–bundle or Seifert-fibered components of the cut manifold, not the guts.

The next lemma addresses the first point for the manifold $(S^3 - L) \backslash\backslash B$. We will call a normal square a *nontrivial square* if it bounds more than one vertex on each side.

Lemma 2.7   *Let L be a link with a reduced, prime, alternating diagram. The following nontrivial squares in the checkerboard polyhedra of $S^3 - L$ give essential annuli in the manifold $(S^3 - L)\backslash\backslash B$:*

   (1)   *a square bounding a string of red bigons, or*

   (2)   *a cycle of fused units, ie a string of squares, each bounding a fused unit, as in Figure 1.*

Conversely, any essential annulus for $(S^3 - L)\backslash\backslash B$ in normal form with respect to the checkerboard polyhedra decomposes into squares with one of the above two forms. A similar statement holds for $(S^3 - L)\backslash\backslash R$, with red and blue surfaces swapped.

Proof   This is essentially due to Lackenby, with the proof contained in [19, Section 5]. We step through the argument.

The first case, of a square bounding a string of red bigons, is dealt with in the first two paragraphs of [19, Section 5]. Each red bigon is a disc with boundary consisting of four edges: two edges lie on blue faces, and two edges lie on vertices of the polyhedron. Each of these can be given a product structure $I \times (\text{arc of } \widetilde{B})$. The parabolic locus P of $(S^3 - L)\backslash\backslash B$ also has a product structure of the form $I \times (\text{arc of } \widetilde{B})$, with the product structure of the red bigon matching that of the parabolic locus. Thus, a neighborhood of the union of the parabolic locus and red bigon faces cuts off an I–bundle component of $(S^3 - L)\backslash\backslash B$. Its boundary is an essential annulus in $(S^3 - L)\backslash\backslash B$. In normal form, this essential annulus will be made up exactly of squares bounding a string of red bigons (the boundary of a neighborhood of red bigons) and trivial squares parallel to vertices. Each nontrivial square bounding red bigons appears in an essential annulus.

In the second case, consider the dashed squares shown in Figure 1, left, or more generally any number of these in a cycle. The gluing on the checkerboard polyhedra glues these along their red faces to the dashed squares shown second from left in Figure 1, and the two collections of squares form an annulus. Together, these cut off a Seifert-fibered solid torus, as shown in Figure 1, right. Thus, this is an essential annulus.

Conversely, in the proof of [19, Theorem 14], Lackenby shows that if there are no red bigons in the diagram, and thus no essential annuli arising from an I–bundle determined by bigons as in case (1), then an essential annulus will be made up of fused units as in Figure 1, left; see also [19, Figures 12 and 13].   □
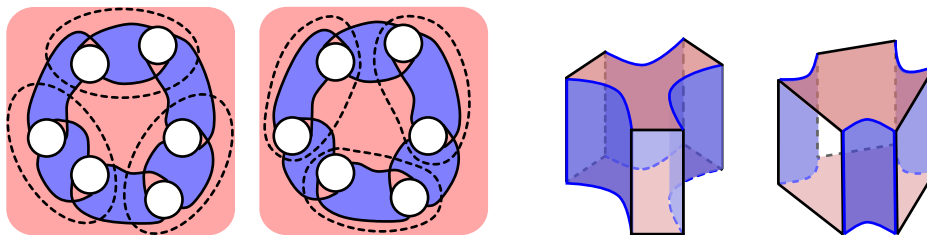
Figure 1: Left: A cycle of three fused units, with dashed squares in each polyhedron. Right: A Seifert-fibered solid torus is built by gluing top faces to top faces and bottom to bottom (ie gluing red faces), with a half-turn on one side.

Lemma 2.8 *Let L be a link with a reduced, prime, alternating diagram and associated checkerboard polyhedra. Then any square in the original checkerboard polyhedra for the link complement $S^3 - L$ gives rise to an embedded annulus in $D(M_B) \backslash\backslash DR$, and this annulus is essential in $D(M_B) \backslash\backslash DR$ if and only if it is a nontrivial square.*

Conversely, any embedded essential annulus in $D(M_B) \backslash\backslash DR$ is obtained by a sequence of an even number of nontrivial squares in the original checkerboard polyhedra.

Proof We prove the "conversely" statement first. It is basically contained in the proof of [8, Lemma 4.10], but we repeat the argument here. By Lemma 2.5, an essential annulus is made up of squares that meet red and blue faces of the polyhedra of $D(M_B) \backslash\backslash DR$. Since we glue by the identity on blue faces, the squares must glue together as shown in Figure 2, left, which is modified from [8]. In that figure, dashed lines indicate squares that lie in one copy of the polyhedron, while straight lines indicate
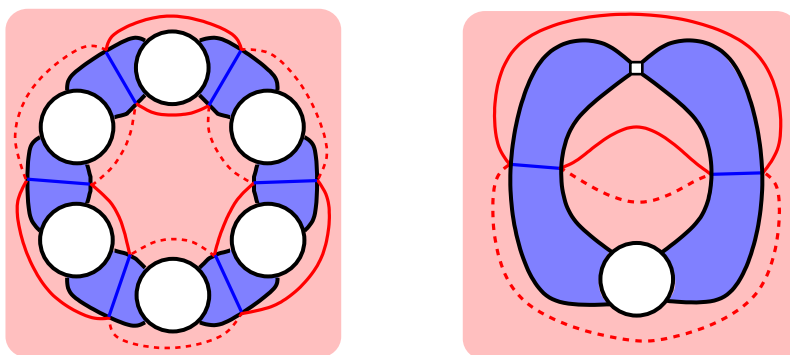

Figure 2: Left: the form of an essential annulus in $D(M_B) \backslash\backslash DR$. Right: if the square encircles a single vertex, the corresponding annulus is inessential.

squares in a second copy, glued to the first by the identity map on blue faces. Note the dashed squares and straight squares glue into an annulus. If there are only two squares and each bounds a region containing a single ideal vertex as in the right figure, then each square making up the annulus is parallel to the ideal vertex shown. After gluing blue faces by the identity, the single ideal vertex becomes an annulus in the parabolic locus. The two squares parallel to that vertex will be parallel to the annulus, and hence not essential.

To prove the first statement, given any square in the polyhedron that encircles more than one ideal vertex on each side, build an annulus in $D(M_B)\backslash\backslash DR$ by taking one copy of the square in each of the two polyhedra that are glued, and gluing by the identity map on blue sides. If the square encircles a single ideal vertex, then the pair of squares glued in $D(M_B)\backslash\backslash DR$ encircle the annulus in the parabolic locus P that comes from the vertex, in particular by gluing the blue faces adjacent to the vertex by the identity map. This is not an essential annulus.

Suppose the annulus is boundary compressible. Then a boundary compression disk has one arc of the boundary on the annulus, and another arc on the red surface. We may cut along the squares, shrink them to ideal vertices and put the boundary compression disk into normal form with respect to these new polyhedra. If the boundary compression disk meets a blue face, then an outermost arc of intersection of the blue face and the compression disk must run from the ideal vertex corresponding to the square to an adjacent edge of the diagram. This contradicts the definition of normal. Thus, the boundary compression disk does not meet a blue face, and thus lies in a single polyhedron. But this means a single arc of the boundary of the compression disk connects opposite sides of the square, red to red. This is impossible because the red faces on opposite sides are not connected (because the diagram is prime). Thus, any such annulus is boundary incompressible. If not boundary parallel, then it is essential. □

In light of Lemma 2.7 and especially Lemma 2.8, determining the guts is analogous to examining squares in the polyhedral decomposition of each manifold. Because the polyhedral decomposition comes from cutting the checkerboard polyhedra of an alternating diagram along squares, finding the guts amounts to analyzing squares in the diagram graph of the alternating link.

The essential annuli that are most important in determining the guts are those that separate hyperbolic pieces from other hyperbolic pieces, or separate hyperbolic pieces from I–bundle or Seifert-fibered pieces. By uniqueness of the JSJ decomposition, these

annuli are unique up to isotopy and pairwise disjoint. There may be additional essential annuli embedded in the Seifert-fibered and I–bundle components of the cut manifolds, and these may not be disjoint from each other. Because we choose to keep the guts only, they do not affect our results. However, we do need to be able to recognize them and discard them.

Lemma 2.9 *Suppose L is a link with reduced, prime, alternating diagram and corresponding checkerboard polyhedra. Let A denote a maximal collection of disjoint essential annuli in $D(M_B) \backslash\backslash DR$. Let C be a component of the polyhedra of $(D(M_B) \backslash\backslash DR) \backslash\backslash A$. Then C gives rise to an I–bundle or Seifert-fibered piece of $(D(M_B) \backslash\backslash DR)$ if and only if C has the combinatorics of the standard diagram of a $(2, q)$–torus link. That is, C is not part of $\mathrm{guts}(D(M_B) \backslash\backslash DR)$ exactly when the red or blue faces of C form a chain of bigons.*

By "maximal" we mean a collection of disjoint essential annuli that is maximal in the sense that there is no other essential annulus that is pairwise disjoint from those already in the collection.

Proof Suppose C has the combinatorics of a $(2, q)$–torus link. Suppose first that the bigon faces of C are all colored red. Then C can be given the structure of an I–bundle: it is homeomorphic to $I \times B_1$, where B_1 is one of the two blue faces of C, with each red face of the form $I \times (\text{arc of } \partial B_1)$. The parabolic locus is also of the form $I \times (\text{arc of } \partial B_1)$. To form $D(M_B) \backslash\backslash DR$, double along the two blue faces. The I–bundle is doubled along $\partial I \times B_1$, forming a Seifert-fibered solid torus $S^1 \times B_1$.

Now suppose that the bigon faces of C are colored blue. Again C can be given the structure of an I–bundle, this time of the form $I \times R_1$, where R_1 is one of the two red faces of C. To form $D(M_B) \backslash\backslash DR$, double along the blue bigon faces. This glues the I–bundle C to an identical I–bundle along blue faces of the form $I \times (\text{arc of } \partial R_1)$, preserving the I–bundle structure. Thus, C yields a component that is not part of the guts.

To prove the converse statement, suppose that C is an ideal polyhedron obtained from cutting one of the ideal polyhedra making up $D(M_B) \backslash\backslash DR$ along a square that forms a larger annulus. Suppose C is not part of $\mathrm{guts}(D(M_B) \backslash\backslash DR)$. Then C belongs to an I–bundle or Seifert-fibered piece of $D(M_B) \backslash\backslash DR$. Suppose C is an I–subbundle of a larger I–bundle Y. The vertical boundary components of the I–bundle Y are vertical

annuli with both boundary components on $\widetilde{DR}$ in $D(M_B)\backslash\backslash DR$, and similarly for C. Because the annuli decompose into squares by Lemma 2.5, the fibers must run parallel to an arc of the blue faces. Because the blue faces glue up to form an essential surface, parallel to one fiber, the blue faces must be a vertical surface, and so each blue face of each annulus is fibered. It follows that each blue face must be of the form $I \times$ arc, and therefore each blue face is a bigon. Now C is an I–subbundle of Y, homeomorphic to a ball with boundary made up of red faces and blue bigons. It follows that C has the combinatorics of a $(2, q)$–torus link made up of a string of blue bigons.

Finally, suppose C belongs to a Seifert-fibered piece Z of $D(M_B)\backslash\backslash DR$. The Seifert-fibering induces a fibering of $\widetilde{DR} \cap Z$. The boundary ∂Z is a torus, and the vertical boundary of C is an annulus that is broken into squares when put into normal form. It follows that, in this case, the red faces of $\widetilde{DR} \cap Z$ are fibered, and hence they form bigons. Then, again, C has the combinatorics of a $(2, q)$–torus link, this time with red bigons. □

We still wish to identify exactly the guts from a diagram. It becomes slightly easier if we consider the manifold

$$M_{BR} := D\big(D((S^3 - L)\backslash\backslash B)\backslash\backslash DR\big)$$

of Proposition 2.1.

Lemma 2.10 *Let L be a link with a reduced, prime, alternating diagram, and associated checkerboard surfaces B and R. The manifold $M_{BR} = D\big(D((S^3 - L)\backslash\backslash B)\backslash\backslash DR\big)$ has the following properties*:

(1) *Any maximal disjoint collection of nontrivial squares in the diagram induces a torus decomposition of M_{BR}, which contains the tori of the JSJ decomposition.*

(2) *Each component of the torus decomposition is built of ideal polyhedra obtained from the original checkerboard polyhedra by cutting along squares.*

(3) *The Seifert-fibered pieces of the decomposition are exactly those obtained by gluing polyhedra with the combinatorics of a $(2, q)$–torus link. All other polyhedra give hyperbolic pieces.*

Proof Note that M_{BR} is obtained by starting with the checkerboard polyhedra of $S^3 - L$, doubling along blue faces, then doubling along red faces. Thus, it has a decomposition into ideal polyhedra with a checkerboard coloring.

For (1), note first that any essential torus can be put into normal form with respect to the polyhedral decomposition. By an Euler characteristic argument, each normal disk making up the torus must be a square. Because the polyhedra have the same combinatorics as the diagram of the alternating link, any collection of essential tori gives a collection of squares.

On the other hand, a nontrivial square in the diagram determines a nontrivial square in the checkerboard polyhedra. When we double across blue and then red faces, the square becomes a torus in M_{BR}. We may cut the checkerboard polyhedra along these squares and collapse the squares to ideal vertices, obtaining new ideal polyhedra. If the torus is compressible, a compressing disk can be put into normal form with respect to these new polyhedra. But, as in the proof of Lemma 2.8, this leads to a contradiction if the square is nontrivial. Also as in the proof of Lemma 2.8, the torus is boundary parallel if and only if the square cuts off a single ideal vertex. Thus, a maximal collection of disjoint nontrivial squares in the diagram bounding more than one crossing on each side gives a maximal collection of embedded essential tori in M_{BR}. By the uniqueness of the JSJ decomposition, this contains the tori of the JSJ decomposition.

Item (2) now follows immediately from (1). Cut along the squares and collapse each square to an ideal vertex to obtain the new polyhedral decomposition.

For (3), note first that if a polyhedron has the combinatorics of a $(2, q)$–torus link, then it has an I–bundle structure of the form $F_1 \times I$, where F_1 is one of the two faces that is not a bigon. When we double and then double, the I–bundle becomes an S^1–bundle, which is doubled across annuli on its boundary in a way that preserves the fiber. Hence, it is Seifert-fibered.

Now suppose a polyhedron C in the complement of the torus decomposition of M_{BR} glues to give a Seifert-fibered component S. Note first that each ideal vertex of C glues under the doubling to a torus in the parabolic locus; hence, the Seifert-fibered component S has infinite fundamental group. Note next that the component admits two involutions: reflection through its intersection with the blue surface and reflection through its intersection with the red surface. It follows from work of Meeks and Scott that the involutions preserve the Seifert fibering [21].

Consider the intersections of the blue and red surfaces with S. These are incompressible surfaces, and hence either vertical or horizontal in S. Suppose first that a component of the blue surface is vertical. Then it is parallel to the fibers of the Seifert fibering. Its intersection with C must have corresponding blue faces also parallel to the fibers.

Because all faces of C are disks, it follows that these blue faces are of the form (arc) $\times I$, or bigon faces. The red meeting the blue cannot also be bigons, else C is formed of four bigons and two ideal vertices, contradicting the fact that the squares in the decomposition were chosen to bound at least two ideal vertices on each side. So the red face must be horizontal in this case. Reflection in the red surface preserves M_{BR}, taking blue surfaces to blue. Hence, C has the combinatorics of a $(2, q)$–torus link with blue bigon faces.

Suppose instead that each component of the blue surface meeting C is horizontal. Note that the torus boundary components of S are fibered. It follows that the (truncated) ideal vertices of C are fibered of the form $\beta \times I$, where β is an arc in the blue face. Then $\partial\beta \times I$ lies in a red face of C. It follows that the red surface must be vertical. Then an argument identical to that above implies that red faces in C are bigons, and again C has the combinatorics of a $(2, q)$–torus link. □

Lemma 2.11 *The manifold $D\big(\mathrm{guts}(D(M_B) \backslash\backslash DR)\big)$ is homeomorphic to*

- $\mathrm{guts}(M_{BR})$, *ie the hyperbolic part of M_{BR},*
- $\mathrm{guts}(M_{RB}) = \mathrm{guts}\, D\big(D((S^3 - L) \backslash\backslash R) \backslash\backslash DB\big)$, *and*
- $D\big(\mathrm{guts}(D(M_R) \backslash\backslash DB)\big)$.

Proof We show first that $\mathrm{guts}(M_{BR})$, the manifold consisting of the hyperbolic components of M_{BR} under the JSJ decomposition, is homeomorphic to $\mathrm{guts}(M_{RB})$. This is straightforward: the manifolds M_{BR} and M_{RB} are both obtained from eight copies of one of the checkerboard polyhedra of the link L, by doubling along red and blue faces, although in different orders. We obtain a homeomorphism $M_{BR} \cong M_{RB}$ by taking a homeomorphism of polyhedra, and then gluing by the identity across faces. Then $\mathrm{guts}(M_{BR}) \cong \mathrm{guts}(M_{RB})$ by the uniqueness of the JSJ decomposition.

Next we show $D\big(\mathrm{guts}(D(M_B) \backslash\backslash DR)\big)$ is homeomorphic to $\mathrm{guts}(M_{BR})$. The argument that $D\big(\mathrm{guts}(D(M_R) \backslash\backslash DB)\big)$ is homeomorphic to $\mathrm{guts}(M_{RB})$ is symmetric. By Lemma 2.10, we obtain $\mathrm{guts}(M_{BR})$ by taking a maximal collection of disjointly embedded nontrivial squares, which bound at least two crossings on both sides, cutting along them and discarding components with the combinatorics of a $(2, q)$–torus link. Then double remaining polyhedra across their red and blue faces. By Lemmas 2.7 and 2.8, we obtain $D\big(\mathrm{guts}(D(M_B) \backslash\backslash DR)\big)$ by first cutting along a collection of squares corresponding to red bigons and cycles of fused units, then cutting along remaining nontrivial squares that are not parallel to one of these squares, nor parallel to a single

ideal vertex, and again discarding components with the combinatorics of a $(2, q)$–torus link by Lemma 2.9.

If there are no fused units in the diagram, then a maximal collection of squares used to create $D\big(\text{guts}(D(M_B)\backslash\backslash DR)\big)$ is a maximal collection of squares used to create $\text{guts}(M_{BR})$, by Lemmas 2.7 and 2.8. To build the guts in both cases, we decompose along these squares and throw away components with the combinatorics of a $(2, q)$–torus link, by Lemmas 2.9 and 2.10. Then we obtain the manifolds by doubling along blue and red faces. These are homeomorphic.

In the case that there is a cycle of fused units, note in the first step of the decomposition of M_B we cut along distinct collections of squares in the two checkerboard polyhedra, and these squares intersect each other; see Figure 1. Hence, we must choose one collection of squares to complete to a maximal collection to form M_{BR}. However, in both polyhedra the exterior of the cycle of fused units has the combinatorics of a $(2, q)$–torus link, so is discarded. And, in both, in the second step of the decomposition there will be two squares within each fused unit that decompose the fused unit into two "units" and a $(2, 3)$–torus link. Thus, only the units remain in the decomposition of $\text{guts}(D(M_B)\backslash\backslash DR)$. Similarly, in the decomposition of $\text{guts}(M_{BR})$, choose squares from the fused units and build a maximal collection of disjoint squares. After discarding $(2, q)$–torus links, at most the units remain in the guts decomposition. Again there is a homeomorphism of polyhedra, and these are identified in both manifolds by doubling along blue and red faces, so the manifolds are homeomorphic. $\qquad\square$

Proof of Proposition 2.1 The homeomorphism result of the proposition is by Lemma 2.11. The fact that the manifolds are obtained by eight copies of polyhedra as claimed follows from Lemma 2.6. $\qquad\square$

Proof of Theorem 2.3 In the hyperbolic structure on $D\big(\text{guts}(D(M_B)\backslash\backslash DR)\big)$, the red surface is preserved by a reflection; thus, as a consequence of Mostow–Prasad rigidity, it must be totally geodesic. Similarly, the blue surface in $D\big(\text{guts}(D(M_R)\backslash\backslash DB)\big)$ is totally geodesic. By Lemma 2.11, these manifolds are homeomorphic, and hence isometric again by Mostow–Prasad rigidity. It follows that red and blue surfaces are totally geodesic in both.

Finally, reflection in the red fixes the red surface pointwise, and takes the blue surface to a totally geodesic surface intersecting the red. Similarly, reflection in the blue fixes the blue pointwise and takes the red to a totally geodesic surface. This is possible only if the two surfaces meet at right angles. $\qquad\square$

3 Topology

The next part of the story is topological. In the previous section, we identified guts by considering squares in the diagram graph. Topologically, cutting along a square can be seen as pulling a tangle out of the diagram. We review here some of the literature on tangle decompositions of alternating links. We will see that the decomposition into guts polyhedra above is related to decompositions into algebraic parts of an alternating link, due in part to Conway [12], Bonahon and Siebenmann [6] and especially Thistlethwaite [31]. However, there are some subtle differences. In this section, we review many of the results discovered by Thistlethwaite, and use them to build ideal polyhedra associated with an alternating link.

Following Thistlethwaite, we define a *tangle* to be a pair (X, T), where X is homeomorphic to S^3 with a finite number of balls removed and the set $T \subset X$ is a 1–manifold, properly embedded in X, such that, for every 2–sphere component F of ∂X, $\partial T \cap F$ consists of four points. This generalizes the typical definition of a 2–tangle, in which X is a ball and T is a 1–manifold inside the ball meeting ∂X in four points. Figure 3 shows three different examples of tangles using this more general definition.

A tangle (X, T) is *trivial* either if X has one boundary component (is a ball) and (X, T) is homeomorphic by a homeomorphisim of pairs to the tangle $(B^3, \text{two unknotted arcs})$, or if X has two boundary components and (X, T) is homeomorphic by a homeomorphism of pairs to the tangle $(S^2 \times I, \text{four unknotted arcs})$ where the endpoints of each arc lie on different boundary components of $S^2 \times I$. A homeomorphism of a tangle with one boundary component to a trivial tangle is well known to be determined by a rational number [12], and thus such a tangle is also called a *rational* tangle.

The *hollow elementary tangle* is homeomorphic to the tangle (X, T) where X has three boundary components and T consists of six unknotted arcs with a pair of arcs between each pair of boundary components of X. Figure 3 shows two trivial tangles and the
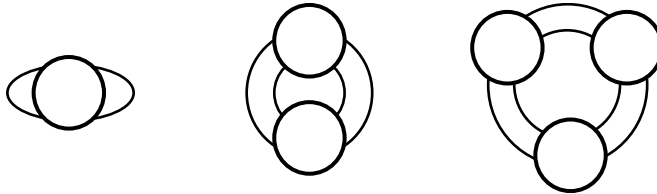

Figure 3: Left to right: a trivial tangle with one boundary component, a trivial tangle with two boundary components, a hollow elementary tangle.

hollow elementary tangle. An *elementary* tangle is obtained from the hollow elementary tangle by gluing a trivial tangle into zero, one or two of its boundary components.

For our purposes here, we define a *Conway sphere* in a tangle (X, T) or link (S^3, L) to be a 2–sphere F in the interior of X meeting T transversely in four points. This differs from Thistlethwaite's definition in [31]: he requires his Conway spheres to be such that neither component of $(X, T) - (F, F \cap T)$ is a trivial tangle with one or two boundary components, forcing the 4–punctured sphere to be essential in $X - T$. We will refer to Thistlethwaite's spheres as *essential* Conway spheres, and use the term Conway sphere to refer to the much more general situation. In any case, we say two Conway spheres are *parallel* if they cobound a trivial tangle with two boundary components.

A note on historical definitions that we will compare to ours: Thistlethwaite defines a link or tangle to be *algebraic* if it is elementary, or if it can be cut along a collection of essential Conway spheres into elementary tangles. For a tangle (X, T) (or a link (S^3, L)), Bonahon and Siebenmann consider the double cover $\widetilde{X}$ of X branched over T [6]. Any essential Conway sphere lifts to an essential torus, and any algebraic tangle lifts to a graph manifold.

It follows by [23; 31] that (S^3, L) contains a maximal finite collection of pairwise disjoint and nonparallel essential Conway spheres $F_1, \dots, F_n$, and this collection is unique outside of elementary tangles. The *algebraic part* of (S^3, L), defined by Thistlethwaite in [31], is the union of the closure of components of $S^3 - \bigcup F_i$ that are elementary.

In [23], Menasco showed that, within an alternating link diagram, essential Conway spheres can have one of two forms, visible or hidden, corresponding to Figure 4.

Definition 3.1 For a given alternating link diagram, a *visible Conway sphere* intersects the plane of projection in a simple closed curve meeting the link diagram transversely in four points. We also require that a visible Conway sphere bounds at least two crossings on each side.

In the case of a hidden essential Conway sphere, the diagram of the link always resembles that of the Borromean rings, with four tangles added, and the hidden Conway sphere meets the plane of projection in two curves. By [31, Proposition 5.1], a visible essential Conway sphere is visible in any alternating diagram of the link. Consequently, a hidden essential Conway sphere is hidden in any alternating diagram of the link;
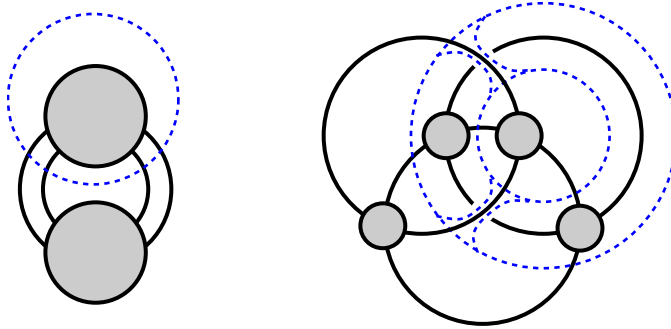
Figure 4: Left: the dashed line shows the intersection of a visible Conway sphere with the link diagram. Right: a hidden Conway sphere intersects the projection plane in two concentric circles, and has two saddles where the two overstrands cross.

see also [15]. For purposes of this paper, we may completely ignore hidden essential Conway spheres. However, we will need to consider visible ones, both essential and inessential. For example, by Definition 3.1, the boundary sphere of a trivial tangle (rational tangle) with at least two crossings in a link diagram is a visible Conway sphere.

Definition 3.2 Let $F_1, \ldots, F_n$ be a maximal, pairwise disjoint and nonparallel collection of visible Conway spheres in a reduced, prime, alternating diagram D. The *visible algebraic part* of D is the union of components of $S^3 - \bigcup F_i$ that are elementary. The diagram D is *visibly algebraic* if all components of $S^3 - \bigcup F_i$ are elementary.

Note that the visible algebraic part differs from Thistlethwaite's algebraic part in two important ways. First, the two differ on diagrams that resemble the Borromean rings. The visible algebraic part will not contain tangles as shown in Figure 4, right, but Thistlethwaite's algebraic part will contain such tangles. Second, the two differ in the presence of a visible *inessential* Conway sphere that bounds a rational tangle that is
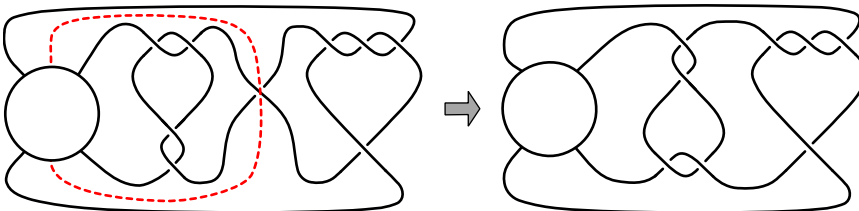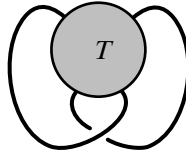

Figure 5: Left: an inessential crossing. Right: the crossing can be removed.

Figure 6: The crossing closure of tangle T.

not a subset of a larger algebraic tangle. Thistlethwaite will completely ignore these rational tangles, but we include them in our visible algebraic part.

A tangle diagram (X, T) is a regular projection of a tangle onto a plane of projection (a 2–sphere), with over- and under-crossing information added to the projection of T. A crossing x in a tangle diagram is *inessential* if there exists an arc α on the plane of projection with $\partial \alpha$ lying on the same component of ∂X and such that α meets T exactly in the point x; see Figure 5, which is adapted from [31]. Note that we may perform a flype to move the crossing to be adjacent to ∂X, then isotope two points of ∂T on ∂X to remove the crossing as in Figure 5, right. A tangle diagram is *reduced* if it contains no inessential crossings.

Definition 3.3 Let (X, T) be a tangle with a reduced, prime, alternating diagram. Attach to each component of ∂X the trivial tangle with one boundary component whose diagram has a single crossing, as in Figure 6. Since T is an alternating tangle diagram, the four points in $T \cap \partial X$ alternate as endpoints of over-crossing and under-crossing arcs of T. Thus, for each added crossing as in Figure 6, we can choose its sign so that the diagram of the resulting link is alternating. Such an alternating link is called the *crossing closure* of the tangle (X, T).

Definition 3.4 (tangle polyhedra) Let L be a link with a reduced, prime, alternating diagram D. Define the *tangle polyhedra* associated with L as follows:

If D is visibly algebraic, then define the *tangle polyhedra* to be the empty set.

If D admits no visible Conway sphere, then define the *tangle polyhedron* to be the checkerboard polyhedron for D.

Otherwise, cut D along a maximal collection of pairwise disjoint, nonparallel, visible Conway spheres $F_1, \ldots, F_n$. Remove the visible algebraic part. What remains consists of a nonempty collection of tangles. For each, reduce the tangle diagram to remove all inessential crossings. Next, form the crossing closure of each tangle, giving a

new collection of alternating link diagrams that are tangle closures of nonalgebraic tangles. Finally, the *tangle polyhedra* are the checkerboard polyhedra of the new reduced alternating link diagrams, taking one checkerboard polyhedron from each pair.

Example 3.5 We provide here a few examples of tangle polyhedra for different diagrams:

  (1) By definition, the tangle polyhedra of any visibly algebraic link is the empty set. This includes 2–bridge knots, Montesinos knots and more complicated algebraic links. The polyhedra of this paper do not give useful information for these links; see the discussion in Section 5.4.

  (2) The usual diagram of the Borromean rings admits no visible Conway spheres. Thus, the tangle polyhedra consist of an ideal octahedron, which agrees with the checkerboard polyhedron, as described in Thurston's notes [33].

  (3) A *weaving knot* $W(p,q)$ is the alternating knot or link with the same projection as the standard closed p–braid $(\sigma_1 \dots \sigma_{p-1})^q$ diagram of the torus knot or link $T(p,q)$. See Section 5.2 for more details on weaving knots. For $p, q \geq 3$, $W(p,q)$ admits no visible Conway spheres; thus, again, their tangle polyhedra consist of an ideal polyhedron with the same combinatorics as the diagram of the weaving knot.

  (4) Take a weaving knot diagram, as above, but replace one crossing by a rational tangle with at least two crossings. By Thistlethwaite's definition of the algebraic part of an alternating link, the resulting link has no algebraic part. However, the *visible* algebraic part of this link, as in Definition 3.2, consists of that rational tangle. Removing it and taking the crossing closure of the result gives back the original weaving knot diagram. Thus, the tangle polyhedra of the weaving knot with a crossing replaced by a rational tangle agree with the tangle polyhedra of the original weaving knot.

In general, replacing any crossing of a diagram by a rational or algebraic tangle does not affect the tangle polyhedra of the result.

Theorem 3.6 *Let L be a link with a reduced, prime, alternating diagram. The tangle polyhedra associated with a given diagram of L are well defined and independent of choice of alternating diagram of L. Therefore, they are a link invariant.*

Proof By the proof of the Tait flyping conjecture [24], any two alternating diagrams of L differ by a finite sequence of flypes. We will show that a single flype does not

affect the tangle polyhedra. It follows that any finite sequence of flypes does not affect the tangle polyhedra of L.

We consider the cases in Definition 3.4 for the reduced, prime, alternating diagram D of L. If D admits no visible Conway sphere, then D does not admit flypes. Suppose D admits a flype along a visible Conway sphere F at a crossing c. We can assume that F is part of the maximal collection of pairwise disjoint, nonparallel, visible Conway spheres for D, as F can be chosen first. If D is visibly algebraic, then, by definition, it remains so after the flype. Before the flype, c is removed in one of two ways: either it lies in the visible algebraic part of D, or it is removed as an inessential crossing with respect to the tangle inside F. After the flype, c is again removed in one of these ways. Thus, following Definition 3.4, we obtain the same collection of nonalgebraic tangles before and after the flype.

So a flype does not change any of the diagrams of the alternating links used to construct the tangle polyhedra. Therefore, the tangle polyhedra form a link invariant. $\square$

Theorem 3.7 *Let L be a link with a reduced, prime, alternating diagram. Any choice of a maximal collection of disjoint squares determines visible Conway spheres and tangle polyhedra on the one hand, and guts polyhedra on the other. Then the associated tangle polyhedra and guts polyhedra are identical.*

Proof By Definition 2.2, the guts polyhedra are obtained by cutting the checkerboard polyhedra associated with the diagram of L along a maximal collection of disjoint squares. The squares that have been cut become ideal vertices. By Lemma 2.9, any component with the combinatorial form of a $(2, q)$–torus link is discarded. The remaining components are the guts polyhedra.

On the other hand, we claim that the tangle polyhedra are also obtained by considering a maximal collection of disjoint squares. For a prime, alternating link, the projection graph of the reduced, alternating diagram and the checkerboard polyhedral graph are the same. Hence, by separating the diagram of L into tangles along a maximal collection of disjoint squares, we get reduced, alternating tangle diagrams that do not admit a visible Conway disk, as defined in [31; 32]. By the classification of alternating tangles in [32], these are exactly the tangles obtained by separating the diagram of L along visible Conway spheres. Hence, separating the diagram of L along squares as in Definition 2.2 or along visible Conway spheres as in Definition 3.4 results in the same set of reduced alternating tangle diagrams.

The visible algebraic part consists of the union of tangles that are either trivial or elementary. Note in Figure 3 that the elementary tangles have a diagram with the combinatorics of a $(2, q)$–torus link. It follows that we remove exactly the same portion of the diagram to form guts polyhedra and tangle polyhedra. In the case of the tangle polyhedra, we take the crossing closure, inserting a crossing into each square. This causes the associated checkerboard polyhedra to have an ideal vertex exactly in the location of the square, which is exactly where the guts polyhedra have an ideal vertex. Thus, the combinatorial polyhedra are identical. □

Corollary 3.8 *For a prime, alternating link L:*

- *The guts polyhedra for L give a link invariant.*
- *The tangle polyhedra admit a right-angled ideal hyperbolic structure.*

4 Combinatorics

The third part of the story is the combinatorics of the diagram graph, which has already played a role in establishing the correspondence between guts polyhedra and tangle polyhedra.

Start with a reduced, twist-reduced, prime, alternating diagram of a link L. This has a 4–valent projection graph $\Gamma(L)$, which may have bigons, and a planar dual graph $\Gamma^*(L)$. A k–circuit is a simple closed curve composed of k edges of a graph. Here we will consider only 4–circuits on $\Gamma^*(L)$ arising from a reduced, twist-reduced, prime, alternating link diagram. We say that a 4–circuit of $\Gamma^*(L)$ is *trivial* if it bounds a single crossing of L on either side, and otherwise it is *nontrivial*.

To avoid ambiguity, we will refer to the diagram of a trivial tangle with either one or two boundary components as a *rational tangle diagram*.

Definition 4.1 Two 4–circuits are *crossing-parallel* if they differ only by passing on opposite sides of a single crossing, as in Figure 7. Two 4–circuits A and B are *parallel* if there is a sequence of 4–circuits $A_1 = A, A_2, \ldots, A_n = B$, with A_j crossing-parallel to A_{j+1} for $j = 1, \ldots, n-1$.

We will consider a nontrivial 4–circuit on the projection plane for $\Gamma(L)$. Capping off by disks on either side of the projection plane, the 4–circuit gives an embedded 4–punctured sphere, which is a visible Conway sphere.
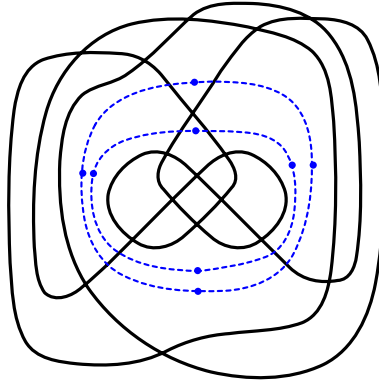
Figure 7: Two crossing-parallel 4–circuits, shown as dashed lines. Although the 4–circuits share two edges, we sketch one pushed slightly inside the other.

Lemma 4.2 *Let A and B be 4–circuits in $\Gamma^*(L)$ with corresponding 4–punctured spheres $\bar{A}$ and $\bar{B}$. Then the following are equivalent*:

(1) *A and B are parallel.*

(2) *$\bar{A}$ and $\bar{B}$ are ambient isotopic in $S^3 - L$.*

(3) *A and B cobound a rational tangle diagram.*

Proof If A and B are parallel, then there exists a sequence of crossing-parallel 4–circuits between them. These determine a sequence of embedded 4–punctured spheres, each pair of which encloses a single crossing of the diagram. The region enclosed is homeomorphic to $S_4 \times I$, where S_4 denotes the 4–punctured sphere. Thus, we have an ambient isotopy from one side of the crossing to the other. Putting these together gives the ambient isotopy from $\bar{A}$ to $\bar{B}$. Hence, (1) implies (2).

If $\bar{A}$ and $\bar{B}$ are ambient isotopic, then they cobound a trivial tangle with two boundary components. We can represent this isotopy by a rational tangle diagram, as pointed out in the remark after [31, Corollary 3.2]. Thus, (2) implies (3).

By [31, Corollary 3.2], if A and B cobound a rational tangle diagram, then it is either unreduced or has no crossings. Thus, the original unreduced alternating diagram is obtained by adding one crossing at a time, adjacent to the 4–circuit A (or B), and so A and B are parallel. Hence, (3) implies (1). $\square$

If a 4–circuit gives a visible Conway sphere that bounds a rational tangle diagram, then that 4–circuit is parallel to a trivial 4–circuit, which bounds one crossing. However,

the trivial 4–circuit inside a rational tangle diagram is not uniquely determined. Thus, by Lemma 4.2, 4–circuits A and B are parallel if and only if they cobound a rational tangle diagram, but such a pair may not be uniquely determined by the tangle diagram.

Definition 4.3 A pair of parallel 4–circuits A and B is called a *maximal bounding pair* if A and B cobound a rational tangle diagram τ, and there do not exist parallel 4–circuits A' and B' that cobound a rational tangle diagram τ' which contains τ as a subtangle. Two maximal bounding pairs $\{A, B\}$ and $\{A', B'\}$ are *disjoint* if they cobound disjoint rational tangle diagrams.

Definition 4.4 Let L be a link with a reduced, twist-reduced, prime, alternating diagram. For all pairwise disjoint maximal bounding pairs of 4–circuits in L, remove all crossings between each pair by a corresponding homeomorphism of each rational tangle. Thus, each rational tangle diagram with one boundary component is replaced by a single crossing, and all crossings are removed in every rational tangle diagram with two boundary components. In the resulting diagram, some 4–circuits that were not parallel before may now be parallel. In that case, repeat the process, removing all crossings between pairwise disjoint maximal bounding pairs of 4–circuits. Because each move reduces the number of crossings, the process eventually terminates. We call this *rational reduction* of the diagram L. The final diagram is *rationally reduced*.

In Figure 8, left, two disjoint maximal bounding pairs of 4–circuits are shown in blue, and two 4–circuits that are not in a maximal bounding pair are shown in red. We use
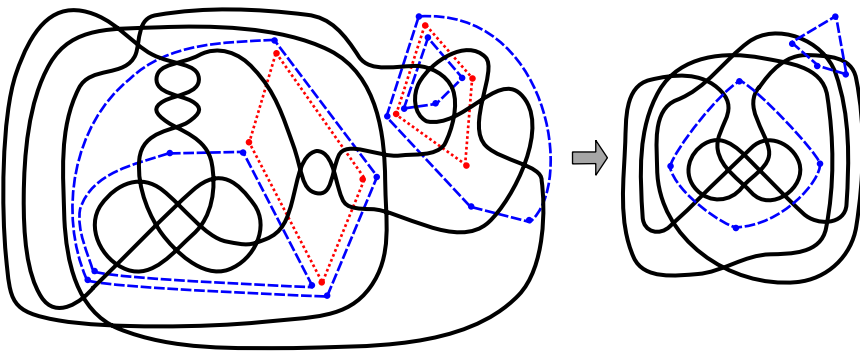

Figure 8: Left: Two disjoint maximal bounding pairs of 4–circuits are shown (long dashed lines, in blue). Two additional 4–circuits that are not in a maximal bounding pair are shown (short dotted lines, in red). Right: Rational reduction eliminates all crossings between both maximal bounding pairs of 4–circuits.

these two maximal bounding pairs to obtain a rationally reduced diagram in Figure 8, right.

Definition 4.5 A *prismatic 4–circuit* is a 4–circuit γ such that no two edges of $\Gamma(K)$ that meet γ share a vertex in $\Gamma(K)$.

It follows from this definition that a prismatic 4–circuit is nontrivial. Conversely, we have the following:

Lemma 4.6 *Each nontrivial 4–circuit of a rationally reduced diagram is a prismatic 4–circuit.*

Proof If not, the 4–circuit meets edges that share a vertex, so the 4–circuit is adjacent to a crossing. But then the diagram is not rationally reduced because there exists a pair of crossing-parallel 4–circuits. □

A combinatorial polyhedron P is a cell complex on S^2 that can be realized as a 3–dimensional convex polyhedron. Steinitz proved that a graph can be realized as the 1–skeleton of such a convex polyhedron if and only if the graph is a 3–connected simple planar graph [30]. A combinatorial polyhedron is realizable as a right-angled hyperbolic polyhedron if there exists an ideal hyperbolic polyhedron with the same combinatorial structure as P and with all dihedral angles $\frac{\pi}{2}$.

Theorem 4.7 (Andreev's theorem for 4–valent right-angled ideal polyhedra) *A 4–valent combinatorial polyhedron admits a realization as a right-angled ideal hyperbolic polyhedron if and only if it has no nontrivial 4–circuits. The realization is unique up to isometry of $\mathbb{H}^3$.*

Proof This special case follows almost immediately from the version of Andreev's theorem given by Atkinson [3, Theorem 2.1]. Let P be a 4–valent combinatorial polyhedron and let Γ denote its 1–skeleton. We step through the necessary and sufficient conditions of that theorem:

(1) P has at least six faces.

(2) Every vertex has degree 3 or 4.

(3) For any triple of faces of P, (F_i, F_j, F_k), such that $F_i \cap F_j$ and $F_j \cap F_k$ are edges of P with distinct endpoints, $F_i \cap F_k = \varnothing$.

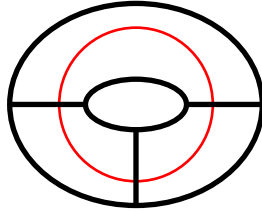(4) P has no prismatic 4–circuits.

Figure 9: The case that F_i and F_k intersect in an edge.

Since P is a combinatorial polyhedron, Steinitz's theorem implies that Γ is a 3–connected simple planar graph. Since Γ is also 4–valent, it follows from the census of knots and links by crossing number (see eg [29]) that Γ has at least six vertices. An Euler characteristic argument implies P must have at least eight faces; hence, conditions (1) and (2) always hold.

Now, if P has no nontrivial 4–circuits then (4) holds by Lemma 4.6. We only need to show that (3) is always satisfied.

Let (F_i, F_j, F_k) be a triple of faces such that $F_i \cap F_j$ and $F_j \cap F_k$ are edges of P with disjoint endpoints, and suppose by way of contradiction that $F_i \cap F_k$ is nonempty.

Case 1 $(F_i \cap F_k$ contains an edge) Then there exists a simple closed curve C that intersects exactly these three edges of P, as shown in Figure 9. Let G be the portion of the graph of P in a disk bounded by C, and let $G' = G \cup C$ be a new graph obtained by adding three edges and three vertices lying on C. Then G' has three vertices of degree 3 and all other vertices of degree 4. This implies that the sum of all degrees of vertices of G' is an odd number. But the sum of all degrees of vertices equals twice the number of edges, which is even: a contradiction.

Case 2 $(F_i \cap F_k$ contains a vertex) In this case we can construct a nontrivial 4–circuit taking the dual edges near the crossing, contradicting the assumption.

The contradictions in both cases imply that P satisfies condition (3) above, and the result follows from [3, Theorem 2.1].

Conversely, suppose P admits a realization as a right-angled ideal hyperbolic polyhedron, and hence satisfies the four conditions above. If P has a nontrivial 4–circuit which is not prismatic, then, using an argument similar to that in Lemma 4.6, this would contradict condition (3). Hence, all nontrivial 4–circuits in P are prismatic, so then condition (4) implies that there are no nontrivial 4–circuits. □

Lemma 4.8 *Let Γ be the 4–valent planar projection graph of a reduced, twist-reduced, prime, alternating link diagram K. Then Γ admits a realization as a right-angled ideal hyperbolic polyhedron if and only if it has no nontrivial 4–circuits. The realization is unique up to isometry of $\mathbb{H}^3$.*

Proof If Γ is a polyhedral graph, then Theorem 4.7 implies it is realized as a right-angled ideal hyperbolic polyhedron if and only if it has no nontrivial 4–circuits. It remains to show that if Γ is not a polyhedral graph, then it has a nontrivial 4–circuit.

By Steinitz's theorem, Γ is a polyhedral graph if and only if it is a 3–connected simple planar graph. Suppose Γ is not simple. The projection graph of a reduced, twist-reduced, prime, alternating link diagram is simple if and only if it has no bigons. If Γ has a bigon, then Γ has a nontrivial 4–circuit encircling the bigon.

Suppose Γ is not 3–connected. Then a curve running through the two vertices that disconnect Γ can be pushed slightly off those vertices to give a nontrivial 4–circuit, using the fact that the diagram is prime. $\qquad\square$

Definition 4.9 (compare to Atkinson [4, Section 3.1]) Let P be a 4–valent planar graph with no bigon regions. If γ is a prismatic 4–circuit for the dual graph P^*, we define *P split along γ*, denoted by $P \setminus\!\setminus \gamma$, as follows: Choose a planar embedding of P. Form two new graphs P_{int} and P_{ext}, where P_{int} (respectively P_{ext}) consists of all edges and vertices of P in the bounded (respectively unbounded) component of $\mathbb{R}^2 - \gamma$, such that P_{int} and P_{ext} each have four 1–valent vertices which were incident to γ. Let $\overline{P}_{\text{int}}$ (respectively $\overline{P}_{\text{ext}}$) be the 4–valent graph obtained by taking the edges
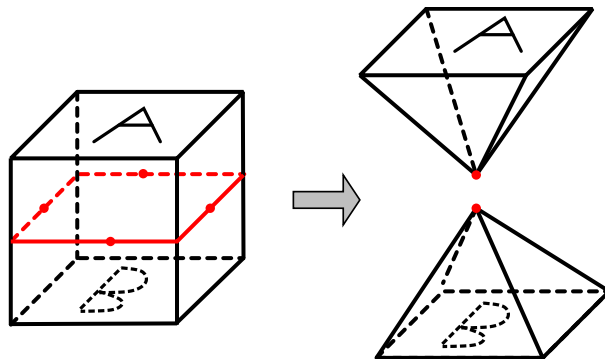

Figure 10: A polyhedron P is split along a prismatic 4–circuit γ (whose dual 4–circuit is shown in the center, in red) to obtain $P \setminus\!\setminus \gamma$, as in Definition 4.9.

from each of the 1–valent vertices, and attaching them to a single vertex chosen to lie in the unbounded (respectively bounded) region of $\mathbb{R}^2 - \gamma$. Then $P \backslash\!\backslash \gamma$ consists of the disjoint union of $\overline{P}_{\text{int}}$ and $\overline{P}_{\text{ext}}$. See Figure 10.

Definition 4.10 (Andreev polyhedra) Start with a reduced, twist-reduced, prime, alternating link diagram L. Let $\Gamma(L)$ be the projection graph of its rationally reduced diagram. Split $\Gamma(L)$ iteratively along nontrivial 4–circuits into graphs that either

  (i)   have exactly one vertex,

  (ii)   have nontrivial 4–circuits, or

 (iii)   have no nontrivial 4–circuits.

We discard all graphs in case (i). For graphs in case (ii), we repeat this process as needed: rationally reduce the corresponding link diagram, and then split along nontrivial 4–circuits as above. Because each move reduces the number of vertices, the process eventually terminates. Finally, the only remaining graphs have no nontrivial 4–circuits. By Lemma 4.8, each such graph admits the structure of a right-angled ideal hyperbolic polyhedron. The resulting set of right-angled ideal hyperbolic polyhedra are called the *Andreev polyhedra* associated to L.

Theorem 4.11 *The Andreev polyhedra are identical to the tangle polyhedra and the guts polyhedra.*

Proof Let D be a reduced, twist-reduced, prime, alternating link diagram. We will prove that Definitions 3.4 and 4.10 agree for D. Rational reduction, as in Definition 4.4, repeatedly replaces all rational tangle diagrams with one boundary component with a single crossing, and removes all crossings in a rational tangle diagram with two boundary components. A visibly algebraic link diagram D is rationally reduced to a 1–crossing diagram, which is discarded in both cases.

We proceed by induction on nontrivial 4–circuits in $\Gamma(D)$. By Lemma 4.2, every set of parallel nontrivial 4–circuits corresponds to a visible Conway sphere. Hence, D admits no visible Conway sphere if and only if $\Gamma(D)$ has no nontrivial 4–circuits. In this case, the two checkerboard polyhedra for D are both its Andreev polyhedra and its tangle polyhedra.

Proceeding inductively, for Andreev polyhedra, we split $\Gamma(D)$ along a nontrivial 4–circuit, and obtain either right-angled polyhedral graphs or graphs with fewer nontrivial

4–circuits that are then rationally reduced. In the latter case, the equivalence with
tangle polyhedra follows by the induction hypothesis. In the former case, we claim
that these right-angled polyhedra are also tangle polyhedra for *D*.

To obtain tangle polyhedra, we cut *D* along visible Conway spheres, remove the
visible algebraic part and inessential crossings, use crossing closures to form reduced
alternating diagrams and then take their checkerboard polyhedra. The crossing closure
makes each checkerboard polyhedron have an ideal vertex exactly where we cut along
the visible Conway sphere, which is the same as splitting Γ along the corresponding
nontrivial 4–circuit. The only difference is when rational reduction occurs: for tangle
polyhedra, the tangles are reduced before taking their crossing closures; for Andreev
polyhedra, we split and rationally reduce each alternating link diagram repeatedly, as
needed, discarding rationally reduced unknots. In both cases, what remains are reduced
alternating diagrams obtained by taking the crossing closure of each nonalgebraic
tangle cut along nontrivial 4–circuits. Thus, the resulting combinatorial polyhedra are
identical.

By Theorem 3.7, these are also the same as the guts polyhedra. □

5 Right-angled volume

In this section, we use the guts/tangle/Andreev polyhedra to define a new geometric
link invariant, which gives a lower bound on the volume of the link.

Definition 5.1 Let *L* be a link with a reduced, twist-reduced, prime, alternating
diagram. The *right-angled volume* $\mathrm{vol}^{\perp}(L)$ is defined to be twice the sum of the
volumes of the right-angled guts polyhedra, or, equivalently by Theorem 4.11, twice
the sum of the volumes of the tangle polyhedra, or twice the sum of the volumes of the
Andreev polyhedra. If the set of such polyhedra is empty, we define $\mathrm{vol}^{\perp}(L) = 0$.

For example, if *L* denotes the standard alternating diagram of the Borromean rings,
the only guts polyhedron is a regular ideal octahedron. Therefore, $\mathrm{vol}^{\perp}(L) = 2v_{\mathrm{oct}}$,
where $v_{\mathrm{oct}} \approx 3.66386$ is the volume of the regular ideal octahedron.

On the other hand, if *L* is any visibly algebraic link, as in Example 3.5(1), $\mathrm{vol}^{\perp}(L) = 0$.

The three equivalent definitions of $\mathrm{vol}^{\perp}(L)$ imply different properties: using tangle
polyhedra we prove the invariance of $\mathrm{vol}^{\perp}(L)$ (Theorem 5.2), using guts polyhedra we

prove the lower bound for the volume of $S^3 - L$ (Theorem 5.3) and using Andreev polyhedra we provide a diagrammatic expression for $\mathrm{vol}^\perp(L)$ (Theorem 5.4).

Theorem 5.2 *If L is any prime, alternating link, then $\mathrm{vol}^\perp(L)$ is a link invariant.*

Proof Using the tangle polyhedra of L to obtain $\mathrm{vol}^\perp(L)$, invariance of the polyhedra follows from Theorem 3.6. The uniqueness of their volume follows from Theorem 4.7. □

Theorem 5.3 *For any hyperbolic alternating link L with hyperbolic volume $\mathrm{vol}(L)$,*

$$\mathrm{vol}^\perp(L) \leq \mathrm{vol}(L).$$

Proof Here, we consider $\mathrm{vol}^\perp(L)$ in terms of the guts polyhedra of L. For a reduced, prime, alternating diagram of L, the guts polyhedra inherit a hyperbolic structure with geodesic faces meeting at right angles, by Theorem 2.3.

A theorem of Agol, Storm and Thurston [2, Theorem 9.1] states that, for a hyperbolic 3–manifold N with embedded π_1–injective surface Σ,

$$\mathrm{vol}(N) \geq \tfrac{1}{2} v_{\mathrm{tet}} \| D(N \backslash\backslash \Sigma) \| = \tfrac{1}{2} \mathrm{vol}\big(D(\mathrm{guts}(N \backslash\backslash \Sigma))\big).$$

Here, v_{tet} is the volume of a regular ideal tetrahedron, $\|\cdot\|$ denotes Gromov norm, Theorem 9.1 of [2] gives the inequality, and the equality is the definition of the Gromov norm.

We apply this result twice, to surfaces B and DR, which implies

$$\begin{aligned} \mathrm{vol}(L) &\geq \tfrac{1}{2} \mathrm{vol}\big(D(\mathrm{guts}((S^3 - L) \backslash\backslash B))\big) = \tfrac{1}{2} \mathrm{vol}(D(M_B)) \\ &\geq \tfrac{1}{4} \mathrm{vol}\big(D(\mathrm{guts}(D(M_B) \backslash\backslash DR))\big). \end{aligned}$$

The manifold $D\big(\mathrm{guts}(D(M_B) \backslash\backslash DR)\big)$ is built by gluing eight copies of the guts polyhedra, glued by the identity along red and blue faces. Thus, this gives the desired result. □

Theorem 5.4 *Let L be a prime, alternating link, given by a reduced, twist-reduced, prime, alternating diagram. Let K be its rationally reduced diagram, as in Definition 4.4.*

(1) *If K has five or fewer crossings, then $\mathrm{vol}^\perp(K) = 0$.*

(2) *If K admits no nontrivial 4–circuits, then $\mathrm{vol}^{\perp}(K) = 2\,\mathrm{vol}(P(K))$, where $P(K)$ is the checkerboard polyhedron for K, with a right-angled ideal hyperbolic structure.*

(3) *Otherwise, split K along nontrivial 4–circuits to obtain a set of alternating tangles whose crossing closures form alternating link diagrams K_i. Repeatedly, as needed, rationally reduce each K_i and apply steps (1)–(3). Let $\{T_i\}$ be the resulting set of reduced nonalgebraic tangles and let $T_i^{\times}$ denote the crossing closure of T_i, as in Figure 6. Then*

$$\mathrm{vol}^{\perp}(L) = \sum_i \mathrm{vol}^{\perp}(T_i^{\times}).$$

Proof For (1), any alternating diagram with five or fewer crossings is visibly algebraic.

For (2), the claim follows by Lemma 4.8. In this case, the two checkerboard ideal polyhedra $P(K)$ are exactly the tangle polyhedra of K.

For (3), we follow the procedure in Definition 4.10. By the proof of Theorem 4.11, the T_i are the tangles whose crossing closures form the tangle polyhedra. The inductive proof gives a way to find the tangle diagrams starting from the link diagram L by repeated rational reduction and splitting. □

Example 5.5 For the Borromean link L, its reduced alternating diagram satisfies condition (2) of Theorem 5.4. Hence, $\mathrm{vol}^{\perp}(L) = \mathrm{vol}(L)$.

Example 5.6 Let τ_1, τ_2 and τ_3 be the tangles shown in Figure 11. Let K be the alternating link obtained by inserting τ_1 into each of the three inner boundary components of τ_2, and then inserting the resulting tangle into the boundary of τ_3. Note K is rationally reduced.

Using Theorem 5.4, we compute $\mathrm{vol}^{\perp}(K)$. Following step (3), we repeatedly split K into alternating diagrams. For both τ_1 and τ_3, the crossing closure is the knot 8_{18}, and
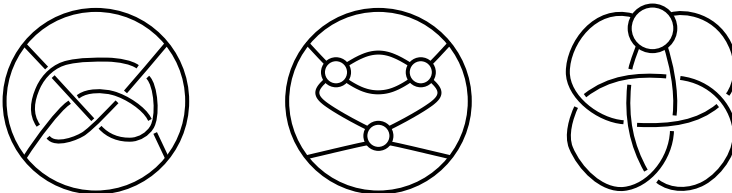

Figure 11: The tangles τ_1, τ_2 and τ_3 used in Example 5.6.

the repeated crossing closure of τ_2 is the figure-eight knot. Thus, we obtain alternating links K_i for $1 \leq i \leq 5$ such that four of the K_i are diagrams of 8_{18}, and the other one is the figure-eight knot diagram. The figure-eight knot is visibly algebraic, and can be rationally reduced to an unknot. Hence, we obtain four crossing closures of tangles $T_i^\times$ in step (3) of Theorem 5.4, and each of these four is the knot 8_{18}. Thus, $\mathrm{vol}^\perp(K) = 4\mathrm{vol}^\perp(8_{18})$. We compute $\mathrm{vol}^\perp(8_{18})$ exactly in Example 5.7 below.

5.1 Computing $\mathrm{vol}^\perp(L)$

We now provide an explicit algorithm to compute $\mathrm{vol}^\perp(L)$ from a reduced, prime, alternating diagram of L. Applying Theorem 5.4, we get a set of reduced nonalgebraic tangles T_i. We can then apply Theorem 5.8, below, to explicitly compute each $\mathrm{vol}^\perp(T_i^\times)$, and hence $\mathrm{vol}^\perp(L)$.

We will compute $\mathrm{vol}^\perp(T_i^\times)$ by dividing right-angled polyhedra into well-understood pieces. Figure 12 shows one such piece, which is a $\frac{3}{4}$–ideal tetrahedron with one vertex at ∞, the other two ideal vertices on the boundary of the same hemisphere on $\mathbb{C} \subset \partial \mathbb{H}^3$, and the finite vertex at the point with maximum Euclidean height on that hemisphere. This is the double of what Schläfli called an *orthoscheme*.

In [25], Milnor computed the volume of the $\frac{3}{4}$–ideal tetrahedron $\mathcal{T}$ of Figure 12. Let θ denote the dihedral angle between the two vertical faces of $\mathcal{T}$ that meet at the vertical edge lying over the finite vertex. By Milnor's calculation, the volume is
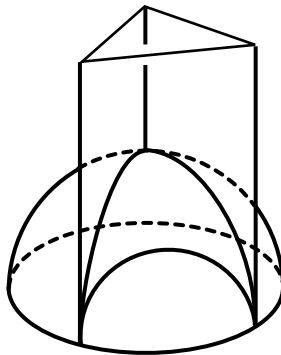

Figure 12: A $\frac{3}{4}$–ideal tetrahedron with ideal vertices at ∞ and on the boundary of a hemisphere, and with finite vertex at the Euclidean maximum of that hemisphere.
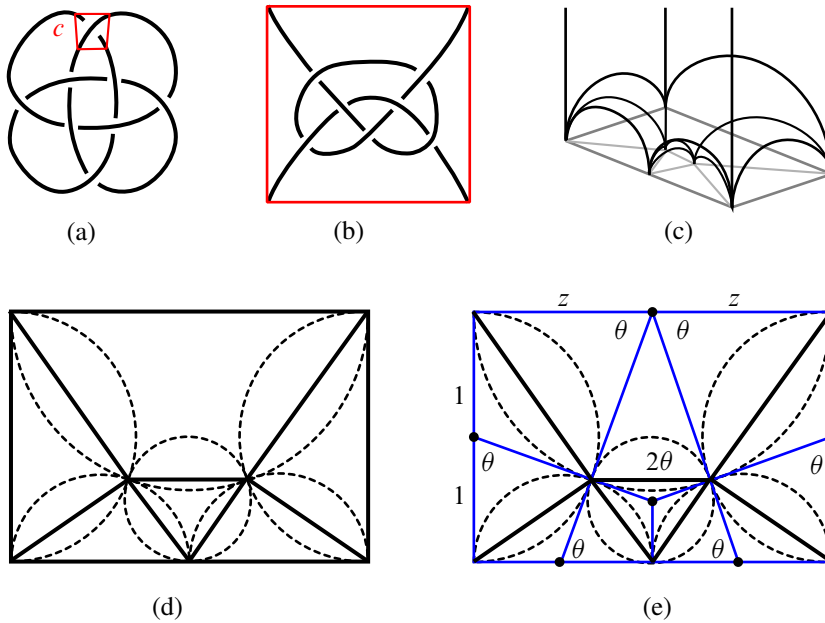
Figure 13: Decomposition of the right-angled polyhedron associated to 8_{18}. (a) Crossing c is chosen to be the ideal vertex at ∞. (b) Diagram now with c at infinity. (c) Geometry of right-angled polyhedron, with faces in $\mathbb{H}^3$ and c at ∞. (d) Circles making up faces of the polyhedron, lying in a rectangle. (e) Circles plus projection of edges of the $\frac{3}{4}$–ideal tetrahedra.

$\mathrm{vol}(\mathcal{T}) = \Lambda\!\left(\frac{1}{2}\theta\right)$, where $\Lambda(\theta)$ is the Lobachevsky function

$$\Lambda(\theta) = -\int_0^\theta \log|2\sin t|\,dt.$$

Example 5.7 We compute $\mathrm{vol}^\perp(L)$ for L the alternating knot 8_{18}. The process is illustrated in Figure 13. Note that the reduced alternating diagram of L is already rationally reduced with no nontrivial 4–circuits.

In Figure 13(a), we choose a crossing c, or alternatively consider c as an ideal vertex of the tangle polyhedron, and take this point to infinity. This is shown in Figure 13(b).

Because the diagram is rationally reduced, we know the tangle polyhedron admits a geodesic right-angled hyperbolic structure. Each of the faces shown in Figure 13(b) will be totally geodesic in this structure, and hence faces define lines and circles on $\partial\mathbb{H}^3$. The polyhedron is shown in 3 dimensions in Figure 13(c), and circles on

$\partial \mathbb{H}^3$ corresponding to the geodesic faces, viewed from the point ∞, are shown in Figure 13(d).

Subdivide the picture into a collection of $\frac{3}{4}$–ideal tetrahedra by adding a vertical edge running from the center of each circle to infinity, and adding faces from this edge to the ideal vertices. The result is shown in Figure 13(e).

Now use symmetry and trigonometry to compute the angles. In this case, six of the angles are the same value θ, six others are $\pi - \theta$, one has angle 2θ and one has angle $\pi - 2\theta$. If we set the size of the rectangle in Figure 13(d) to be $2 \times 2z$, then $\tan\left(\frac{1}{2}\theta\right) = 1/z = \frac{1}{2}z$. Then $\tan\left(\frac{1}{2}\theta\right) = 1/\sqrt{2}$, and $\mathrm{vol}^\perp(L) \approx 12.0461$.

A *right kite* is a kite with two right angles. The geometric data encoded in the rectangle $R(c)$ of Figure 13(e) is completely determined by the tiling of $R(c)$ by right kites, shown in blue lines in Figure 13(e). This follows because the projection of all the $\frac{3}{4}$–ideal tetrahedra to $\partial \mathbb{H}^3$ gives a rectangle tiled by isosceles triangles, which meet in pairs across the edges of the diagram to form right kites. In each kite, right angles are dihedral angles of the right-angled polyhedron; the remaining kite angles are of the form θ and $\pi - \theta$. See Figure 14.

Therefore, we can view the procedure described in Example 5.7 as a geometric realization problem. Namely, the geometric Figure 13(d) is the realization of its combinatorial graph, shown with solid lines in Figure 13(d), which can be obtained directly from
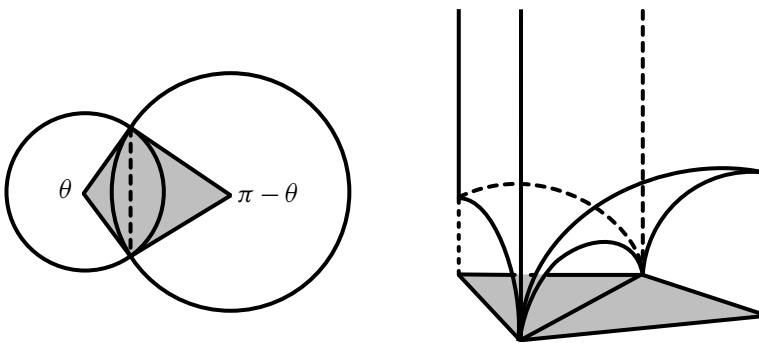

Figure 14: Left: A right kite formed by radii of intersecting circles, meeting at the dashed edge e shown as the short diagonal. The radii meet at right angles; the other two angles of the kite are θ and $\pi - \theta$. Right: An ideal hyperbolic polyhedron is bounded by vertical planes and intersecting hemispheres above a kite, which consists of two $\frac{3}{4}$–ideal tetrahedra.
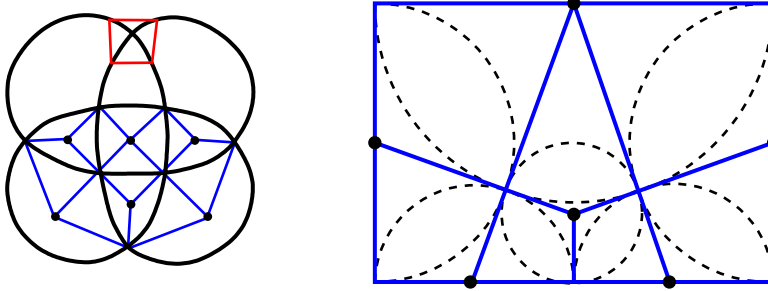
Figure 15: Left: the graph G, shown with blue edges, is obtained from $\Gamma(L)$, as in Theorem 5.8, with the crossing c indicated in the red box. Right: G is realized as a tiling of the rectangle $R(c)$ by right kites.

the diagram in Figure 13(b). We generalize this procedure below, showing that, for appropriate prime, alternating links, the corresponding combinatorial graph can be geometrically realized.

The *central triangulation* of a face of a plane graph is obtained by adding a central vertex to the face, and edges joining the central vertex to all other vertices, triangulating the face.

Theorem 5.8 *Let L be a prime, alternating link, whose link diagram is already rationally reduced and has no nontrivial 4–circuits. Let $\Gamma(L)$ be the projection graph of the link diagram. Fix any crossing c of L, and let $\mathcal{F}(c)$ be the closure of the four faces of $\Gamma(L)$ which meet c. Let G be the graph obtained by taking the central triangulation of each face of $\Gamma(L)$ that does not meet c, excluding the edges in $\Gamma(L)$. Then G can be realized as a Euclidean rectangle tiled by right kites, with one kite k_e for each edge e of $\Gamma(L)$ not in $\mathcal{F}(c)$. Let θ_e and $\pi - \theta_e$ denote the other kite angles of k_e. Then*

$$\mathrm{vol}^{\perp}(L) = 2 \sum_{e \in \Gamma(L) \setminus \mathcal{F}(c)} \Lambda\left(\tfrac{1}{2}\theta_e\right) + \Lambda\left(\tfrac{1}{2}(\pi - \theta_e)\right).$$

We illustrate the graphs in Theorem 5.8 for the knot 8_{18} in Figure 15.

Proof Let $P = P(L)$ be the checkerboard ideal polyhedron of L. Since the diagram of L is already rationally reduced, the 1–skeleton of P is the diagram graph of L, denoted by $\Gamma(L)$. Hence, P is 4–valent and the number of ideal vertices of P equals the number of crossings in L. By Lemma 4.8, P admits a right-angled ideal hyperbolic structure.

We can realize P in $\mathbb{H}^3$ so that the ideal vertex corresponding to the crossing c is ∞. The four faces incident to c are vertical half-planes in $\mathbb{H}^3$ intersecting at right-angles. The faces of P not incident to ∞ are hemispheres which intersect each other and the vertical faces at right-angles. Thus, P is the polyhedron inside the chimney formed by the vertical faces and above the hemispheres, as in Figure 13(c).

Let $R(c)$ denote the rectangle in $\mathbb{C} \subset \partial \mathbb{H}^3$ bounded by lines which are the boundaries of vertical faces of P. Inside $R(c)$, an orthogonal circle pattern is formed by circles which are boundaries of the hemispherical faces of P. The ideal vertices of P, other than ∞, are the points of intersection of four circles, half-circles or lines in $R(c)$, as in Figure 13(d).

Let $\mathcal{G} \subset R(c)$ be the graph whose vertices are the centers of the circles in $R(c)$ and the ideal vertices of P other than ∞, and whose edges are (Euclidean) line segments joining the center of each circle to the ideal vertices lying on that circle. Note that the boundary of the rectangle $R(c)$ consists of edges and vertices of $\mathcal{G}$. Since the ideal vertices of P, other than ∞, lie on the circles, every face of $\mathcal{G}$ is a quadrilateral such that two opposite vertices are centers of intersecting circles, and the other two vertices are the points of intersection. Hence, every face of $\mathcal{G}$ is a kite. The angle of intersection of two hemispheres in $\mathbb{H}^3$ equals the angle of intersection of its boundary circles, which in turn equals the (equal and opposite) angles of the kite formed by the center of the circles and the points of intersection. Since P is right-angled, $\mathcal{G}$ is a rectangle tiled by right kites.

On the other hand, the vertices of G are the vertices of $\Gamma(L)$, other than c, along with the central vertex of each face of $\Gamma(L)$, other than those meeting c. The edges of G are the edges from each central vertex to the vertices of that face. The faces of G are quadrilaterals which correspond to the edges of $\Gamma(L)$ that do not meet c. Each side of $R(c)$ corresponds to the boundary of each of the four faces meeting c. The degree of each vertical polygonal face of P is the degree of the corresponding face. Since the circles in $R(c)$ correspond to the faces of P not adjacent to ∞, this implies that the vertices and edges of $\mathcal{G}$ and G coincide, and hence they are isomorphic as planar graphs.

The volume formula then follows from the result of Milnor [25].   □

5.2 Right-angled volume for weaving knots

We now apply Theorem 5.8 to an infinite family of knots and links. A *weaving knot* $W(p, q)$ is the alternating knot or link with the same projection as the standard closed
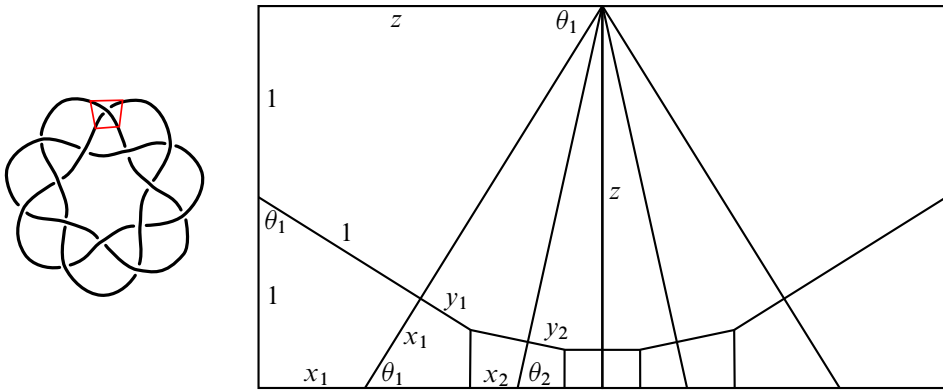
Figure 16: Left: $W(3, 7)$ diagram with chosen crossing. Right: right kite structure for $W(3, 7)$, with certain kite angles and edge lengths labeled.

p–braid $(\sigma_1 \ldots \sigma_{p-1})^q$ diagram of the torus knot or link $T(p, q)$. The knot 8_{18} is the weaving knot $W(3, 4)$. See Table 1 for several other examples of weaving knots. See [9] for more details on weaving knots.

Theorem 5.9 *For all weaving knots $W(3, q)$, we can compute $\mathrm{vol}^{\perp}(W(3, q))$ by an algorithm that requires solving a one-variable polynomial equation.*

Proof Theorem 5.4(1) implies $\mathrm{vol}^{\perp}(W(3, q)) = 0$ for $q \leq 2$. To compute $\mathrm{vol}^{\perp}(W(3, q))$ for $q \geq 3$, we follow the procedure in Theorem 5.8 to obtain its right kite structure. We start with the case $W(3, 2n + 1)$. See Figure 16, which shows a knot diagram for $W(3, 7)$ and its right kite structure, with certain kite angles and edge lengths in a $2 \times 2z$ rectangle. For $W(3, 2n + 1)$, the kite angles are θ_i, and the edge lengths are z and $\{x_i, y_i\}$ for $i = 1, \ldots, n - 1$, extending the pattern shown in Figure 16 for $n = 3$. All the other angles and edge lengths can then be determined immediately from these. Note that for all $W(3, 2n + 1)$, the two kites centered at the bottom are squares.

The formulas below are for $\{x_i, y_i, \theta_i \mid i = 1, \ldots, n - 1\}$, and we define $y_0 = 1$:

$$\tan\left(\tfrac{1}{2}\theta_1\right) = x_1 = \frac{y_1}{x_1} = \frac{1}{z}, \qquad \text{hence} \qquad y_1 = x_1^2 \quad \text{and} \quad z = \frac{1}{x_1};$$

$$\tan\left(\tfrac{1}{2}\theta_i\right) = \frac{y_i}{x_i} = \frac{x_i}{y_{i-1}}, \qquad \text{hence} \qquad x_i^2 = y_i y_{i-1};$$

$$\tan\left(\tfrac{1}{2}(\theta_{i+1} - \theta_i)\right) = \frac{y_i}{z} = x_1 y_i, \qquad \text{hence} \qquad \frac{\tan\left(\tfrac{1}{2}\theta_{i+1}\right) - \tan\left(\tfrac{1}{2}\theta_i\right)}{1 + \tan\left(\tfrac{1}{2}\theta_{i+1}\right)\tan\left(\tfrac{1}{2}\theta_i\right)} = x_1 y_i.$$

This implies

$$x_i\, y_{i+1} - x_{i+1}\, y_i = x_1\, y_i (x_i x_{i+1} + y_i\, y_{i+1});$$

thus,

$$x_i \left(\frac{x_{i+1}^2}{y_i} \right) - x_{i+1}\, y_i = x_1\, y_i (x_i x_{i+1} + x_{i+1}^2),$$

so

$$x_{i+1} = \frac{x_1 x_i\, y_i^2 + y_i^2}{x_i - x_1\, y_i^2}.$$

These equations imply that x_{i+1} can always be expressed by a rational function in just the variable x_1. For example, for all $W(3, q)$, $x_2 = (x_1^5 + x_1^3)/(1 - x_1^4)$. In addition, using the midline of the rectangle, $z + y_{n-1} = 2$, which implies that $\sum x_i = z - 1 = 1/x_1 - 1$. This yields one polynomial equation in x_1, whose solution provides a solution for all edge lengths, x_i and y_i.

For $W(3, 2n)$, the right kite structure extends the pattern shown in Figure 13(e), and we get the same equations as above, except $\sum x_i = \frac{1}{2} z = 1/(2x_1)$.

Finally, the kite angles θ_i can be computed from the edge lengths. By Theorem 5.8, this provides an algorithmic solution for $\mathrm{vol}^{\perp}(W(3, q))$ for each q. □

See Table 1 for numerical computations of $\mathrm{vol}^{\perp}(W(p, q))$ for several small values of p and q. The equality for the Borromean link L is exact: all four of its right kites are squares, so $\mathrm{vol}^{\perp}(L) = 16$ and $\Lambda\left(\frac{1}{4}\pi\right) = \mathrm{vol}(L)$. The exact equality for $W(4, 4)$ was proved in [14].

5.3 Asymptotically sharp volume bounds

Our results in [8; 10] imply that the lower bound from right-angled volume is asymptotically sharp for many sequences of alternating links. Using our results above, we prove that we can remove the "no cycle of tangles" condition from [8, Theorem 1.4; 10, Theorem 6.7].

Let $\mathcal{W}$ be the infinite square weave and let $\mathcal{Q}$ be the triaxial link, which are biperiodic alternating links discussed in [8; 10]. Let W and Q be the respective toroidally alternating quotient links. Let $v_{\mathrm{tet}} \approx 1.01494$ and $v_{\mathrm{oct}} \approx 3.66386$ be the hyperbolic volumes of the regular ideal tetrahedron and the regular ideal octahedron, respectively. Let $c(K)$ denote the crossing number of K.

$W(p, q) = L$	$\mathrm{vol}^\perp(L)$	$\mathrm{vol}(L)$
$W(3, 2) = 4_1$	0	2.0299
$W(3, 3) =$ Borromean link	7.3277	7.3277
$W(3, 4) = 8_{18}$	12.0461	12.3509
$W(4, 3) = 9_{40}$	14.6554	15.0183
$W(3, 5) = 10_{123}$	16.2758	17.0857
$W(3, 6) = L12a1882$	19.4287	21.6316
$W(3, 7) = 14a19470$	24.2126	26.0544
$W(4, 4) = L12a2008$	24.0922	24.0922

Table 1: Right-angled volumes for several low-crossing weaving knots.

Theorem 5.10 *Let K_n be any sequence of alternating hyperbolic link diagrams which satisfy **Følner convergence almost everywhere**, as in [10, Definition 6.1], to $\mathcal{W}$ and $\mathcal{Q}$, respectively. Then*

$$K_n \xrightarrow{F} \mathcal{W} \implies \lim_{n \to \infty} \frac{\mathrm{vol}(K_n)}{c(K_n)} = \lim_{n \to \infty} \frac{2\pi \log \det(K_n)}{c(K_n)} = \frac{\mathrm{vol}((T^2 \times I) - W)}{c(W)} = v_{\mathrm{oct}},$$

$$K_n \xrightarrow{F} \mathcal{Q} \implies \lim_{n \to \infty} \frac{\mathrm{vol}(K_n)}{c(K_n)} = \lim_{n \to \infty} \frac{2\pi \log \det(K_n)}{c(K_n)} = \frac{\mathrm{vol}((T^2 \times I) - Q)}{c(Q)} = \frac{10}{3} v_{\mathrm{tet}}.$$

Proof For links without a cycle of tangles, the proofs of [8, Theorem 1.4] and [10, Theorem 6.7] relied on a lower volume bound coming from the checkerboard polyhedra of K_n, given an ideal right-angled hyperbolic structure. Now, we use instead the guts polyhedra of K_n, whose volume is $\mathrm{vol}^\perp(K_n)$, which is a lower volume bound by Theorem 5.3. Since neither $\mathcal{W}$ nor $\mathcal{Q}$ contains a cycle of tangles, any cycles of tangles in K_n must be in $G(K_n) - G_n$. Thus, if we use the guts polyhedra, the proofs are otherwise unchanged. □

Corollary 5.11 *The lower bound, $\mathrm{vol}^\perp(L)$, is asymptotically sharp; ie there exists a sequence of alternating hyperbolic links K_n such that*

$$\lim_{n \to \infty} \frac{\mathrm{vol}^\perp(K_n)}{\mathrm{vol}(K_n)} = 1.$$

Proof By Theorem 5.10, there exist sequences of alternating links K_n and K_n' such that

$$\lim_{n \to \infty} \frac{\mathrm{vol}^\perp(K_n)}{c(K_n)} = \lim_{n \to \infty} \frac{\mathrm{vol}(K_n)}{c(K_n)} = v_{\mathrm{oct}}, \quad \lim_{n \to \infty} \frac{\mathrm{vol}^\perp(K_n')}{c(K_n')} = \lim_{n \to \infty} \frac{\mathrm{vol}(K_n')}{c(K_n')} = \frac{10}{3} v_{\mathrm{tet}}.$$

It follows that, for any sequence K_n such that $K_n \xrightarrow{F} \mathcal{W}$ or $K_n \xrightarrow{F} \mathcal{Q}$,

$$\lim_{n\to\infty} \frac{\mathrm{vol}^{\perp}(K_n)}{\mathrm{vol}(K_n)} = 1. \qquad\qquad \square$$

For an example of such a sequence, let $K_n = W(p_n, q_n)$ for any $p_n, q_n \to \infty$. Then $K_n \xrightarrow{F} \mathcal{W}$.

5.4 Comparison to other volume bounds

By [2; 19], for any hyperbolic alternating link diagram L with twist number $t(L)$,

$$(1) \qquad\qquad \tfrac{1}{2} v_{\mathrm{oct}}(t(L) - 2) \le \mathrm{vol}(L).$$

Both this lower bound and the one we obtain from $\mathrm{vol}^{\perp}(L)$ are equalities for the Borromean link. In general, the bound in (1) seems to provide information about the volume of the "algebraic" part of L. By contrast, $\mathrm{vol}^{\perp}(L)$ gives no information on volumes of the algebraic part, but seems to give better estimates when the algebraic part is "small." For example, by Theorem 5.10, there are many families of alternating links K_n with $\mathrm{vol}(K_n)/c(K_n) \to v_{\mathrm{oct}}$ such that $t(K_n)/c(K_n) \to 1$. For such alternating links K_n, including weaving links, $\mathrm{vol}^{\perp}(K_n)$ will be at least twice the lower bound in (1).

For the examples in Table 1, $\mathrm{vol}^{\perp}(L)$ beats all previous diagrammatic lower volume bounds. However, as discussed in Section 3, for any visibly algebraic link L, there are no tangle polyhedra, so $\mathrm{vol}^{\perp}(L) = 0$. For example, any Montesinos link L, whose hyperbolic volume can be arbitrarily large, has $\mathrm{vol}^{\perp}(L) = 0$. Similarly, for any arborescent link L with no hidden Conway spheres, $\mathrm{vol}^{\perp}(L) = 0$, but the lower bound in (1) is nonzero. As discussed above, there also exist arborescent links whose alternating diagram does not admit visible Conway spheres, such as the Borromean link B, for which $\mathrm{vol}^{\perp}(B) = \mathrm{vol}(B)$.

It would be useful to be able to combine estimates on algebraic parts of links using (1) with the volume bound of Theorem 5.3. However, at this time our techniques do not allow us to combine the two arguments used to prove the different bounds.

5.5 Right-angled links

We say that a hyperbolic link L is *right-angled* if $S^3 - L$ with the complete hyperbolic structure admits a decomposition into ideal hyperbolic right-angled polyhedra. For

example, the Whitehead link and Borromean link are right-angled alternating links. But $\mathrm{vol}^\perp(L) = \mathrm{vol}(L)$ only for the Borromean link; $\mathrm{vol}^\perp(L) = 0$ for the Whitehead link. Among nonalternating links, the class of fully augmented links is right-angled [11; 28].

Hyperbolic right-angled 3–manifolds have interesting properties. The right-angled decomposition gives an immersed totally geodesic surface in the 3–manifold arising from the faces of the polyhedra. Another property is that their fundamental groups are virtually special [11]. In general, it seems difficult to prove that a hyperbolic 3–manifold is not right-angled. For example, Calegari proved that the knot 8_{20} has no immersed totally geodesic surfaces [7, Corollary 4.6]. This implies that 8_{20} is not right-angled.

Conjecture 5.12 *There does not exist a right-angled knot.*

Together with Theorem 5.3, Conjecture 5.12 would imply that, for any knot K,

$$\mathrm{vol}^\perp(K) < \mathrm{vol}(K).$$

Volume bounds for ideal right-angled polyhedra provide another obstruction for links to be right-angled. By [3], the regular ideal octahedron has the smallest volume among all such polyhedra. Thus, any hyperbolic link L with $\mathrm{vol}(L) < v_{\mathrm{oct}}$ cannot be right-angled; for alternating links L, if $\mathrm{vol}(L) < 2v_{\mathrm{oct}}$, then $\mathrm{vol}^\perp(L) = 0$.

Recently, Vesnin and Egorov [34] enumerated the volumes of ideal right-angled polyhedra with at most 23 faces. Using their enumeration, we have verified Conjecture 5.12 for all knots up to 11 crossings.

Question 5.13 Does there exist a hyperbolic alternating link L, besides the Borromean link, for which $\mathrm{vol}^\perp(L) = \mathrm{vol}(L)$?

Remark 5.14 Since we posted this paper on arXiv, Gan showed that there are exactly three links with two totally geodesic checkerboard surfaces [14]. These are the Borromean link with underlying graph the octahedron, a 4–component link with underlying graph the cuboctahedron (which is $W(4, 4)$ from Table 1) and a 6–component link with underlying graph the icosidodecahedron. These are illustrated in [14, Figure 6]. In particular, there are no knots whose checkerboard surfaces are right-angled totally geodesic, resolving a special case and providing more evidence for Conjecture 5.12. Moreover, for these three links, $\mathrm{vol}^\perp(L) = \mathrm{vol}(L)$, giving two more examples to Question 5.13. See [14, Remark 3.15]. Thus, to extend Theorem 5.3, it is reasonable to conjecture that, for any hyperbolic alternating link L, except for the three links in [14],

$$\mathrm{vol}^\perp(L) < \mathrm{vol}(L).$$

References

[1] **I Agol**, *Lower bounds on volumes of hyperbolic Haken* 3–*manifolds*, preprint (1999) arXiv math/9906182

[2] **I Agol**, **P A Storm**, **W P Thurston**, *Lower bounds on volumes of hyperbolic Haken* 3–*manifolds*, J. Amer. Math. Soc. 20 (2007) 1053–1077 MR Zbl

[3] **C K Atkinson**, *Volume estimates for equiangular hyperbolic Coxeter polyhedra*, Algebr. Geom. Topol. 9 (2009) 1225–1254 MR Zbl

[4] **C K Atkinson**, *Two-sided combinatorial volume bounds for non-obtuse hyperbolic polyhedra*, Geom. Dedicata 153 (2011) 177–211 MR Zbl

[5] **R J Aumann**, *Asphericity of alternating knots*, Ann. of Math. 64 (1956) 374–392 MR Zbl

[6] **F Bonahon**, **L C Siebenmann**, *New geometric splittings of classical knots and the classification and symmetries of arborescent knots*, preprint, 30th year edition (2010) Available at `https://dornsife.usc.edu/assets/sites/1191/docs/Preprints/BonSieb.pdf`

[7] **D Calegari**, *Real places and torus bundles*, Geom. Dedicata 118 (2006) 209–227 MR Zbl

[8] **A Champanerkar**, **I Kofman**, **J S Purcell**, *Geometrically and diagrammatically maximal knots*, J. Lond. Math. Soc. 94 (2016) 883–908 MR Zbl

[9] **A Champanerkar**, **I Kofman**, **J S Purcell**, *Volume bounds for weaving knots*, Algebr. Geom. Topol. 16 (2016) 3301–3323 MR Zbl

[10] **A Champanerkar**, **I Kofman**, **J S Purcell**, *Geometry of biperiodic alternating links*, J. Lond. Math. Soc. 99 (2019) 807–830 MR Zbl

[11] **E Chesebro**, **J DeBlois**, **H Wilton**, *Some virtually special hyperbolic* 3–*manifold groups*, Comment. Math. Helv. 87 (2012) 727–787 MR Zbl

[12] **J H Conway**, *An enumeration of knots and links, and some of their algebraic properties*, from "Computational problems in abstract algebra" (J Leech, editor), Pergamon, Oxford (1970) 329–358 MR Zbl

[13] **D Futer**, **E Kalfagianni**, **J Purcell**, *Guts of surfaces and the colored Jones polynomial*, Lecture Notes in Math. 2069, Springer (2013) MR Zbl

[14] **H-C Gan**, *Alternating links with totally geodesic checkerboard surfaces*, Algebr. Geom. Topol. 21 (2021) 3107–3122 MR Zbl

[15] **J Hass**, **A Thompson**, **A Tsvietkova**, *Tangle decompositions of alternating link complements*, Illinois J. Math. 65 (2021) 533–545 MR Zbl

[16] **W Jaco**, *Lectures on three-manifold topology*, CBMS Reg. Conf. Ser. Math. 43, Amer. Math. Soc., Providence, RI (1980) MR Zbl

[17] **W H Jaco**, **P B Shalen**, *Seifert fibered spaces in* 3–*manifolds*, Mem. Amer. Math. Soc. 220, Amer. Math. Soc., Providence, RI (1979) MR Zbl

[18] **K Johannson**, *Homotopy equivalences of* 3–*manifolds with boundaries*, Lecture Notes in Math. 761, Springer (1979) MR Zbl

[19] **M Lackenby**, *The volume of hyperbolic alternating link complements*, Proc. Lond. Math. Soc. 88 (2004) 204–224 MR Zbl

[20] **F Löbell**, *Beispiele geschlossener dreidimensionaler Clifford–Kleinscher Räume negativer Krümmung*, Ber. Verh. Sächs Akad. Wiss. Leipzig Math.-Phys. Kl. 83 (1931) 167–174 Zbl

[21] **W H Meeks, III**, **P Scott**, *Finite group actions on* 3–*manifolds*, Invent. Math. 86 (1986) 287–346 MR Zbl

[22] **W W Menasco**, *Polyhedra representation of link complements*, from "Low-dimensional topology" (S J Lomonaco, Jr, editor), Contemp. Math. 20, Amer. Math. Soc., Providence, RI (1983) 305–325 MR Zbl

[23] **W Menasco**, *Closed incompressible surfaces in alternating knot and link complements*, Topology 23 (1984) 37–44 MR Zbl

[24] **W Menasco**, **M Thistlethwaite**, *The classification of alternating links*, Ann. of Math. 138 (1993) 113–171 MR Zbl

[25] **J Milnor**, *Hyperbolic geometry: the first* 150 *years*, Bull. Amer. Math. Soc. 6 (1982) 9–24 MR Zbl

[26] **J M Montesinos**, *Seifert manifolds that are ramified two-sheeted cyclic coverings*, Bol. Soc. Mat. Mexicana 18 (1973) 1–32 MR Zbl In Spanish

[27] **J W Morgan**, *On Thurston's uniformization theorem for three-dimensional manifolds*, from "The Smith conjecture" (J W Morgan, H Bass, editors), Pure Appl. Math. 112, Academic, Orlando, FL (1984) 37–125 MR Zbl

[28] **J S Purcell**, *An introduction to fully augmented links*, from "Interactions between hyperbolic geometry, quantum topology and number theory" (A Champanerkar, O Dasbach, E Kalfagianni, I Kofman, W Neumann, N Stoltzfus, editors), Contemp. Math. 541, Amer. Math. Soc., Providence, RI (2011) 205–220 MR Zbl

[29] **D Rolfsen**, *Knots and links*, Math. Lect. Ser. 7, Publish or Perish, Berkeley, CA (1976) MR Zbl

[30] **E Steinitz**, *Polyeder und Raumeinteilungen*, from "Geometries" (F Klein, W Meyer, editors), Encycl. Math. Wiss. 3, Teubner, Leipzig (1922) 1–139

[31] **M B Thistlethwaite**, *On the algebraic part of an alternating link*, Pacific J. Math. 151 (1991) 317–333 MR Zbl

[32] **M Thistlethwaite**, *On the structure and scarcity of alternating links and tangles*, J. Knot Theory Ramifications 7 (1998) 981–1004 MR Zbl

[33] **W Thurston**, *Geometry and topology of three-manifolds*, lecture notes, Princeton Univ. (1980) Available at `http://library.msri.org/books/gt3m/`

[34] **A Y Vesnin**, **A A Egorov**, *Ideal right-angled polyhedra in Lobachevsky space*, Chebyshevskiĭ Sb. 21 (2020) 65–83 MR Zbl

Department of Mathematics, College of Staten Island, City University of New York
Staten Island, NY, United States

Department of Mathematics, College of Staten Island, City University of New York
New York, NY, United States

School of Mathematics, Monash University
Clayton VIC, Australia

`abhijit@math.csi.cuny.edu`, `ikofman@math.csi.cuny.edu`,
`jessica.purcell@monash.edu`